THE GEOLOGICAL SOCIETY OF AMERICA®

# The tempo of continental arc construction in the Mesozoic Median Batholith, Fiordland, New Zealand

**Joshua J. Schwartz[1,*], Keith A. Klepeis[2], Joseph F. Sadorski[1], Harold H. Stowell[3], Andy J. Tulloch[4], and Matthew A. Coble[5]**
[1]DEPARTMENT OF GEOLOGICAL SCIENCES, CALIFORNIA STATE UNIVERSITY NORTHRIDGE, 18111 NORDHOFF STREET, NORTHRIDGE, CALIFORNIA 91330, USA
[2]DEPARTMENT OF GEOLOGY, UNIVERSITY OF VERMONT, 180 COLCHESTER AVENUE, BURLINGTON, VERMONT 05405, USA
[3]DEPARTMENT OF GEOLOGICAL SCIENCES, UNIVERSITY OF ALABAMA, 201 7TH AVENUE, ROOM 2003 BEVILL BUILDING, TUSCALOOSA, ALABAMA 35487, USA
[4]GNS SCIENCE, 764 CUMBERLAND STREET, DUNEDIN 9016, PRIVATE BAG 1930, DUNEDIN 9054, NEW ZEALAND
[5]SCHOOL OF EARTH, ENERGY & ENVIRONMENTAL SCIENCES, STANFORD UNIVERSITY, 397 PANAMA MALL, MITCHELL BUILDING 101, STANFORD, CALIFORNIA 94305, USA

## ABSTRACT

We investigate the temporal record of magmatism in the Fiordland sector of the Median Batholith (New Zealand) with the goal of evaluating models for cyclic and episodic patterns of magmatism and deformation in continental arcs. We compare 20 U-Pb zircon ages from >2300 km$^2$ of Mesozoic lower and middle crust of the Western Fiordland Orthogneiss to existing data from the Median Batholith to: (1) document the tempo of arc construction, (2) estimate rates of magmatic addition at various depths during arc construction, and (3) evaluate the role of cyclical feedbacks between magmatism and deformation during high and low magma addition rate events. Results from the Western Fiordland Orthogneiss indicate that the oldest dates are distributed in northern and southern extremities: the Worsley Pluton (123–121 Ma), eastern McKerr Intrusives (128–120 Ma), and Breaksea Orthogneiss (123 Ma). Dates within the interior of the Western Fiordland Orthogneiss (Misty and Malaspina Plutons, western McKerr Intrusives) primarily range from 118 to 115 Ma and signify a major flux of mafic to intermediate magmatism during which nearly 70% of the arc root was emplaced during a brief, ~3 m.y., interval. The spatial distribution of dates reveals an inward-focusing, arc-parallel younging of magmatism within the Western Fiordland Orthogneiss during peak magmatic activity. Coupled with existing data from the wider Median Batholith, our data show that Mesozoic construction of the Median Batholith involved at least two high-flux magmatic events: a surge of low-Sr/Y plutonism in the Darran Suite from ca. 147 to 136 Ma, and a terminal surge of high-Sr/Y magmatism in the Separation Point Suite from 128 to 114 Ma, shortly before extensional collapse of the Zealandia Cordillera at 108–106 Ma. Separation Point Suite magmatism occurred at all structural levels, but was concentrated in the lower crust, where nearly 50% of the crust consists of Cretaceous arc-related plutonic rocks. Existing isotopic data suggest that the flare-up of high-Sr/Y magmatism was primarily sourced from the underlying mantle, indicating an externally triggered, dynamic mantle process for triggering the Zealandia high–magma addition rate event, with only limited contributions from upper plate materials.

LITHOSPHERE GSA Data Repository Item 2017080 doi:10.1130/L610.1

## INTRODUCTION

Cyclic and episodic patterns of crustal growth are generally believed to have dominated the geologic record for more than 3 b.y. (Bradley, 2011; Voice et al., 2011; Condie and Kroner, 2013). In Phanerozoic orogenic belts, studies of continental arcs often emphasize the non–steady-state character of magmatism whereby episodic and relatively short lived, high magma addition rate (MAR) events significantly contribute to the overall budget of new crust added to the continental lithosphere (e.g., Armstrong, 1988; Kimbrough et al., 2001; Ducea, 2002; Ducea and Barton, 2007; DeCelles et al., 2009). These high-MAR events can exert primary controls on orogenic belts, including widespread thermal and mass transfer from the mantle to the crust, vertical uplift and exhumation, and erosion at the surface (e.g., de Silva at al., 2015; DeCelles and Graham, 2015).

Studies of shallow to mid-crustal plutons and batholiths in the North American and South American Cordilleras have recognized patterns of episodic and cyclic magmatism and deformation that operate on ~30–70 m.y. intervals (Haschke et al., 2002, 2006; DeCelles et al., 2009; DeCelles and Graham, 2015; Paterson and Ducea, 2015; de Silva et al., 2015; Lee and Anderson, 2015; Pepper et al., 2016). At a finer scale, temporal fluctuations in magma supply within arcs appear to be fractal, with episodicity recurring at progressively finer scales (de Silva et al., 2015). Existing models that attempt to explain the episodic nature of arc magmatism commonly invoke either external forcing of arc systems caused by events outside the arc, and/or cyclic processes driven internally by feedbacks between linked tectonic, sedimentary, and magmatic processes (Haschke et al., 2002, 2006; DeCelles et al., 2009; Chapman et al., 2013; Cao et al., 2015; Paterson and Ducea, 2015; Ducea et al., 2015). External forcing can involve a variety of potential processes, including changes in mantle flow patterns, plate reconfigurations due to far-field effects or local processes (e.g., ridge-trench or tectonic collisions), and/or changes in slab dynamics (e.g., slab breakoff or rollback). In contrast, internal feedbacks may involve repeated and linked tectonic and magmatic processes, including underthrusting of foreland or retroarc material into lower crustal parts of arcs, crustal thickening, and loss of mafic and/or ultramafic plutonic roots. A key feature commonly emphasized in internally forced models

*Corresponding author: joshua.schwartz@csun.edu

is the significant role of upper plate materials in triggering episodes of high-volume magmatism. Despite extensive work on arc magmatic tempos, particularly in the last decade, there is currently no consensus on the cause of episodic and cyclical magmatism in arcs. Consequently, a number of processes remain unconstrained, including triggering mechanisms, the rates of magmatic addition to various structural levels (lower, middle, and upper crust), the relative contribution of the mantle versus preexisting crustal sources, and the role of deformation in cyclical and episodic patterns of magmatism.

The complexity of non–steady-state magmatism is perhaps best illustrated in the Mesozoic North American Cordillera arc of the western USA and Mexico, where voluminous shallow- to mid-crustal rocks were generated episodically during various high-MAR events that have distinct geochemical features in different segments of the arc (e.g., Ducea, 2001). For example, in the central Sierra Nevada segment, batholithic rocks are characterized by geochemical and isotopic signatures that point to increasing contributions of recycled crust and lithospheric mantle extracted from deep (>35–40 km) within the arc that appear to be cyclical and peak from ca. 100 to 85 Ma (e.g., Ducea and Barton, 2007; Lackey et al., 2008; DeCelles et al., 2009; Chapman et al., 2013; Cao et al., 2015). Chapman et al. (2013) suggested that in the southern Sierra Nevada segment and further south to the northern Peninsular Ranges, Cretaceous high-flux magmatism resulted from shallowing of the Farallon plate and widespread devolatilization of schistose rocks during a brief, <10 m.y. high-MAR episode (see also Grove et al., 2008 for the northern Peninsular Ranges Batholith). Whereas Chapman et al. (2013) and Grove et al. (2008) emphasized partial melting of supracrustal material at the base of the arc (either from the retroarc or accretionary complex), data from the southern Coast Plutonic Complex (British Columbia) and North Cascades (Washington) show strong depleted-mantle signatures with little evidence for significant supracrustal involvement (Cui and Russell, 1995; Shea et al., 2016). These variations from the Mesozoic North American arc system raise the question of whether the strong upper plate geochemical characteristics in the Sierra Nevada–Salinia–Mojave arc segments reflect cyclical, internally forced processes involving partial melting of fertile continental crust, or simply elevated geothermal gradients resulting from increasing mantle melt influx to the base of the crust controlled by changes in the geometry and geodynamics of the subduction zone (de Silva et al., 2015).

Despite a lack of consensus regarding the causes of episodic fluctuations in arc magmatism, a common feature of internal and external forcing models is that triggering processes occur deep within the arc, in the underlying mantle wedge and/or in a lower crustal, melting, assimilation, storage, and homogenization zone (Hildreth and Moorbath, 1988). Therefore, direct observations of exhumed magmatic arcs, particularly lower crustal arc sections, have the potential to provide insights into the causes of episodic magmatism and the magmatic and residual products produced during high-MAR events.

We investigate temporal patterns of magmatism and deformation along the Mesozoic, paleo-Pacific margin of southeast Gondwana, now isolated and preserved in Zealandia, which records a history of episodic magmatism that operated from the Carboniferous to Early Cretaceous (Mortimer et al., 1999; Mortimer, 2004; Fig. 1). We focus on the exhumed arc root exposed in the Fiordland sector of Zealandia and use SHRIMP-RG (sensitive high-resolution ion microprobe–reverse geometry) dates and zircon trace element data from 20 new samples coupled with existing dates to: (1) document the tempo of arc construction and temporal variations in magmatism along the Mesozoic Gondwana margin; (2) estimate rates of magmatic addition at various structural levels during arc construction; and (3) evaluate the role of cyclical feedbacks between magmatism and deformation, including externally and internally forced processes during high and low MAR events. We show that construction of the Median Batholith involved at least two high-flux and geochemically distinct magmatic events: a surge of low-Sr/Y plutonism in the Darran Suite from ca. 147 to 136 Ma, and a terminal surge of high-Sr/Y magmatism in the Separation Point Suite from 128 to 114 Ma, shortly before extensional collapse of the Zealandia Cordillera, beginning ca. 108–106 Ma. The terminal high flux event in the Separation Point Suite occurred at all structural levels, but was concentrated in the lower crust, where nearly 50% of the crust consists of Cretaceous arc-related plutonic rocks. This phase of magmatism, starting at 128 Ma, reflects a fundamental change in magma composition, with garnet playing a role as either a fractionating or residual phase, and signifies a major transition in internal arc and/or subduction zone dynamics in the Median Batholith. Continentward migration of the arc axis and contraction and/or transpression in Fiordland during the high-MAR event suggest that flattening of the slab and/or changes in subduction zone geometry were associated with triggering the high-flux event. The overall mafic and isotopically juvenile character (Decker, 2016) of the arc root in Western Fiordland also points toward an externally triggered, mantle-generated event with only limited contributions from upper plate materials. We see no evidence that the two Mesozoic surges are related either by internally or externally forced processes, and we suggest that the processes driving them are independent.

## GEOLOGIC SETTING AND PREVIOUS WORK

### Mesozoic Arc in Fiordland, Westland, Stewart Island

The South Island of New Zealand preserves a nearly complete, exhumed section of a Mesozoic Cordilleran-type magmatic arc (Figs. 1–3) (Mortimer et al., 1999). Arc-related plutonic and volcanic rocks were emplaced episodically over a period of ~250 m.y. from the Carboniferous to Early Cretaceous (Fig. 4), and collectively compose the ~10,200 km$^2$ composite Median Batholith (Kimbrough et al., 1993, 1994; Mortimer et al., 1999; Hollis et al., 2004; Tulloch and Kimbrough, 2003; Allibone et al., 2009a, 2009b). The Median Batholith was constructed on the continental margin of the paleo-Pacific margin of Gondwana in what is now the Western Province of New Zealand (Figs. 1A, 1B) (Mortimer et al., 2014). Approximately 70% of the Median Batholith consists of Triassic to Early Cretaceous plutonic rocks that intruded into Carboniferous to Permian igneous rocks and Ordovician metasedimentary rocks. We focus on the Mesozoic components of the Median Batholith in Fiordland, including the Darran Suite and Separation Point Suite, the latter of which was emplaced during a high-MAR event from 128 to 114 Ma. We briefly introduce the Darran Suite and Separation Point Suite. Additional information is included in Tables 1–2.

#### *Darran Suite*

The Darran Suite (sensu Allibone et al., 2009a) consists of calc-alkalic to alkalic-calcic volcanic and plutonic rocks emplaced between ca. 230 and 136 Ma during a prolonged and episodic period of arc magmatism on or east of the convergent Gondwana margin (Figs. 1A, 1B) (Kimbrough et al., 1994; Tulloch and Kimbrough, 2003; Scott and Palin, 2008; Scott et al., 2009; Allibone et al., 2009a). It consists of a belt ~300 km long and 15 km wide that occupies much of the outboard (eastern) side of the Median Batholith. The inboard and outboard portions of the batholith are separated by intrabatholith faults and shear zones such as the Grebe mylonite zone and Gutter shear zone (Fig. 2) (Allibone and Tulloch, 2008; Scott et al., 2011). Although previous studies have mapped Darran Suite rocks within the inboard side of the Median Batholith, recognition of plutons of unambiguous Darran Suite intruding the Western Province

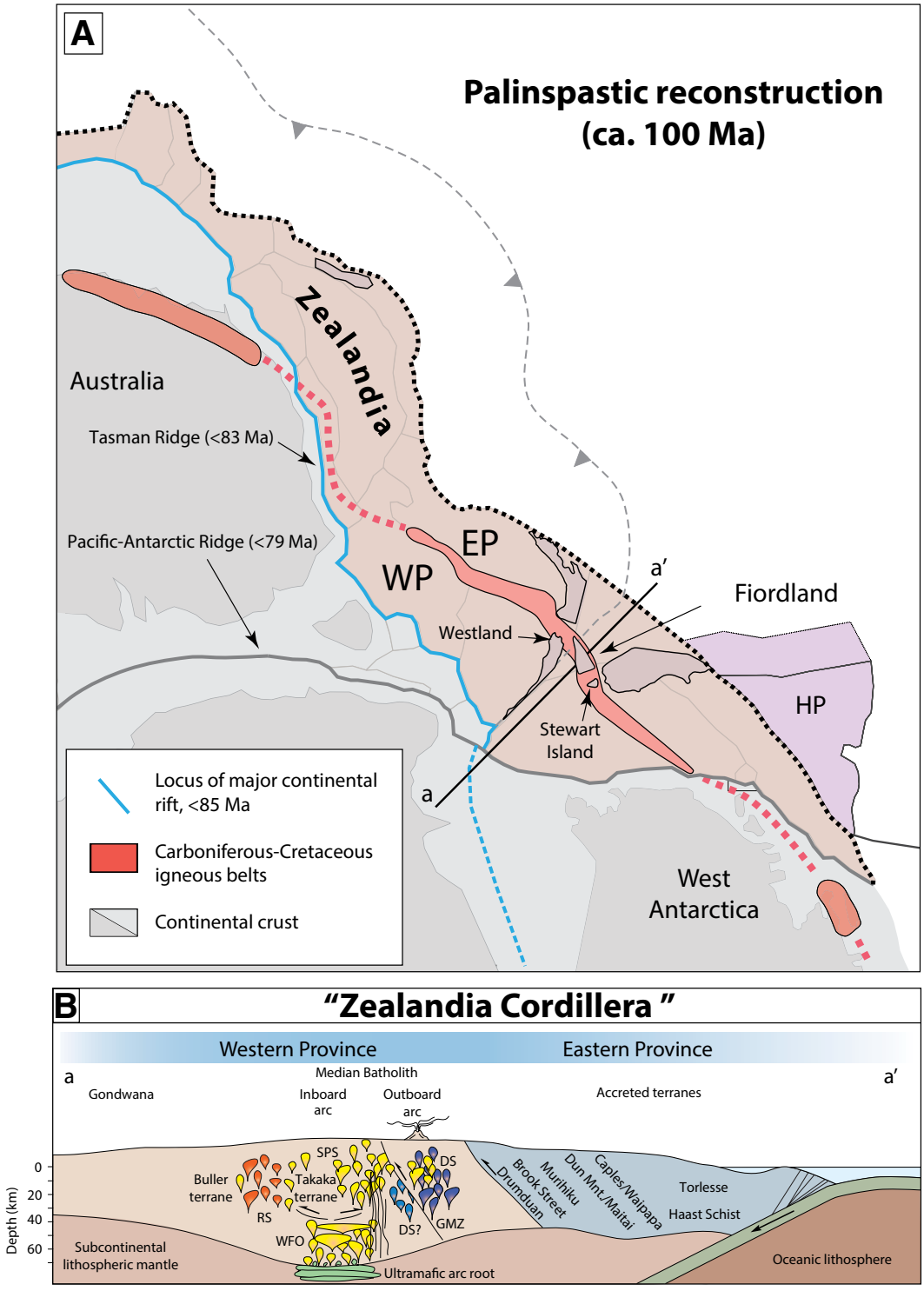


**Figure 1. Palinspastic reconstruction of the Gondwana margin and Zealandia at the termination of arc magmatism ca. 100 Ma (modified after Mortimer, 2008). Westland, Stewart Island, and Fiordland typify parts of the shallow- to deep-crustal components of the Cordilleran-type magmatic arc (red shaded belt) prior to extensional orogenic collapse and rifting. (B) Reconstructed cross section of Zealandia Cordillera prior to termination of arc magmatism. Modified after Mortimer et al. (2014) and Kern et al. (2016). DS—Darran Suite; EP—Eastern Province; GMZ—Grebe mylonite zone; HP—Hikurangi Plateau; RS—Rahu Suite; SPS—Separation Point Suite; WFO—Western Fiordland Orthogneiss; WP—Western Province.**

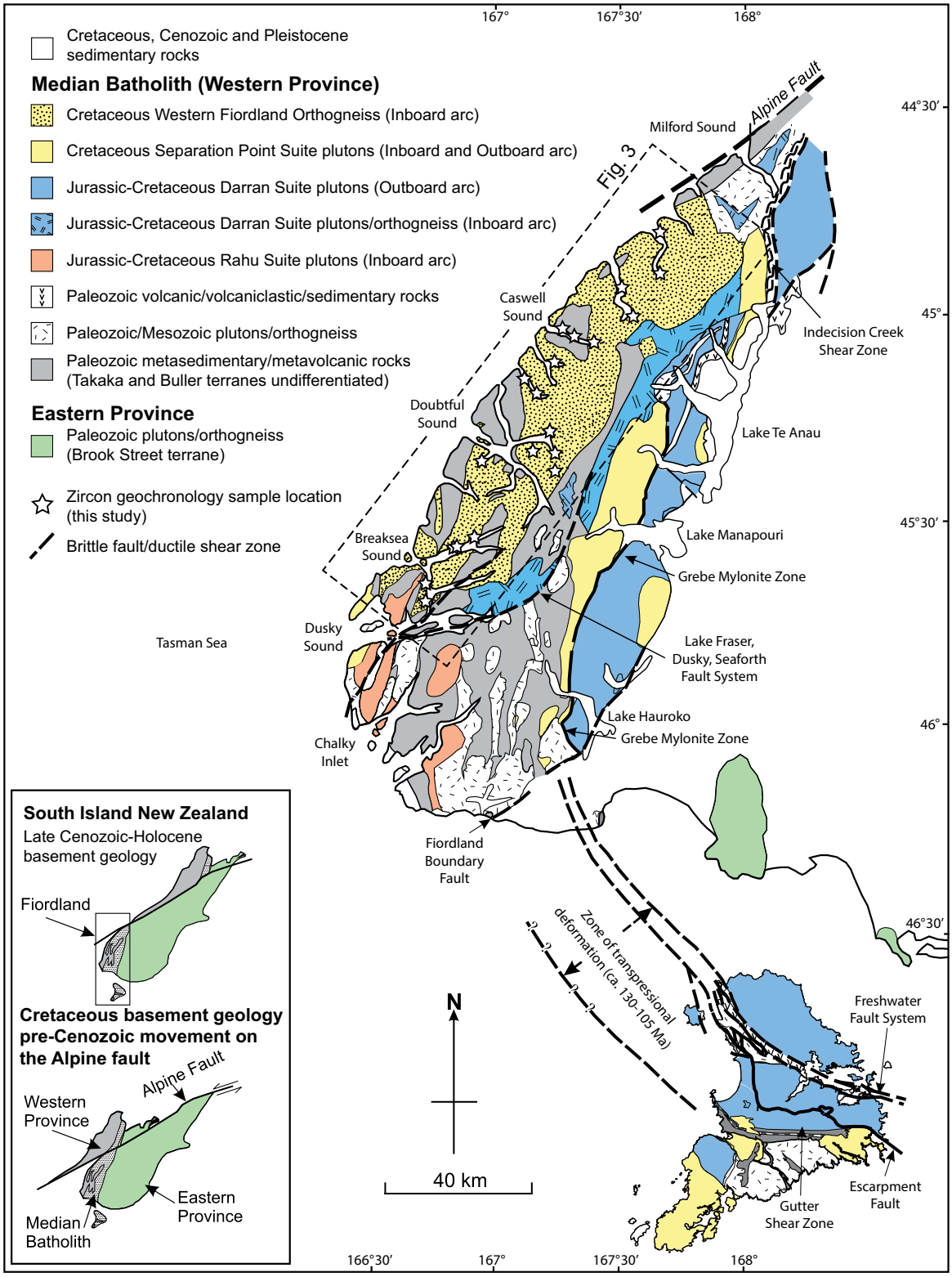


**Figure 2. Geologic map of the Median Batholith (after Allibone and Tulloch, 2008). Sample locations in the Western Fiordland Orthogneiss are indicated by white stars. Inset shows Cretaceous reconstruction of the South Island prior to late Cenozoic–Holocene movement along the Alpine fault (after Klepeis et al., 2004).**

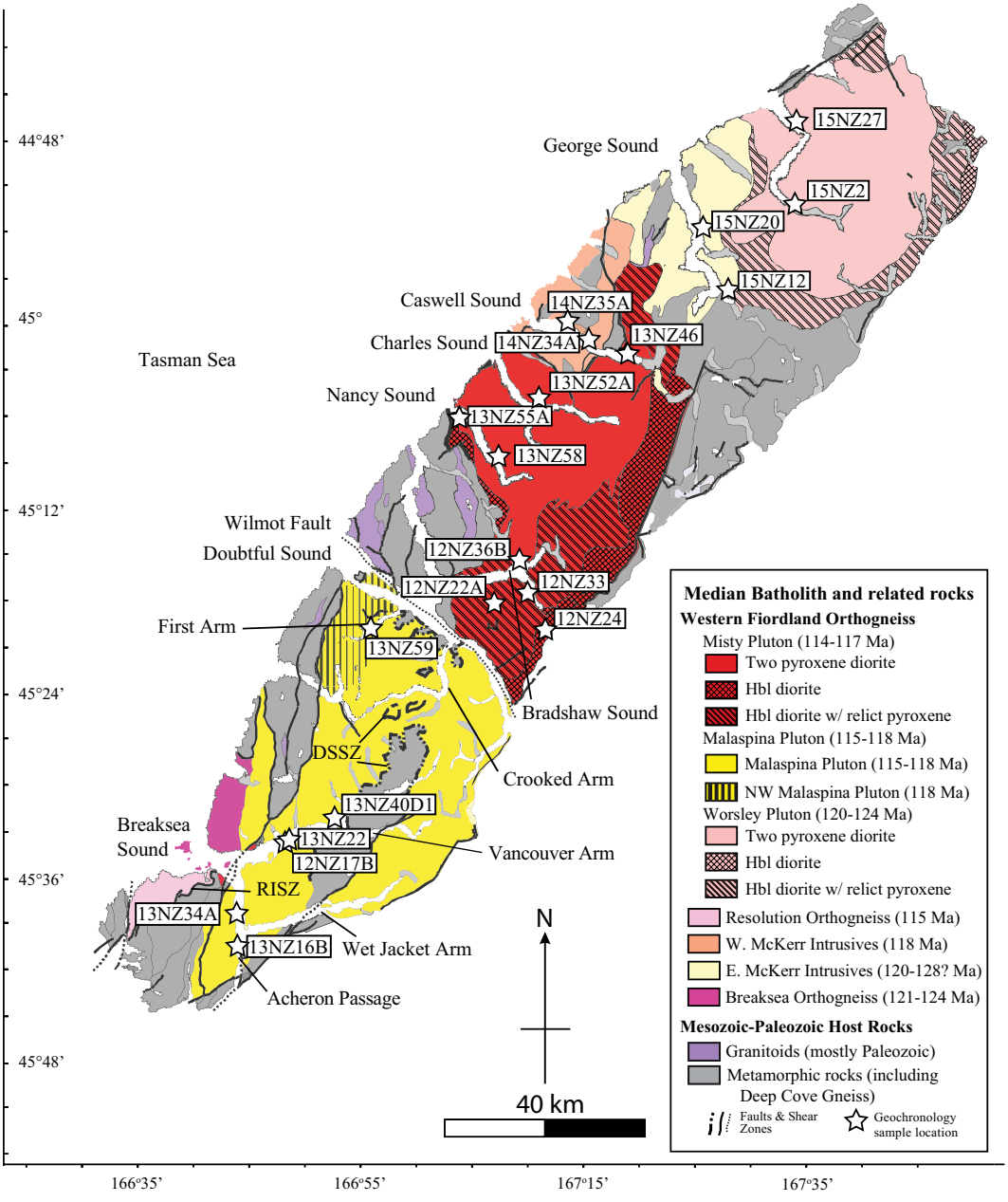


**Figure 3. Geologic map of western Fiordland, New Zealand, focusing on the Western Fiordland Orthogneiss and surrounding prebatholithic rocks (after Allibone et al., 2009b). Sample locations are shown by white stars. DSSZ—Doubtful Sound shear zone; RISZ—Resolution Island shear zone; Hbl—hornblende.**

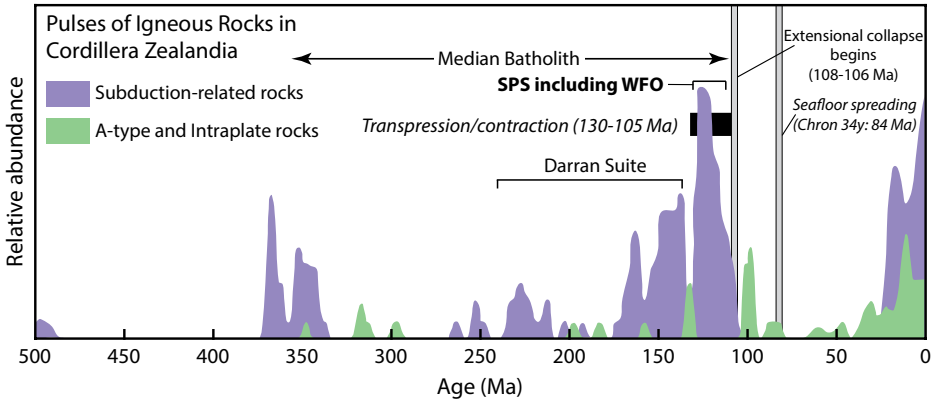


**Figure 4. Plot of number of crystallization dates versus time showing pulses of igneous rocks in Zealandia (after Mortimer and Campbell, 2014). Data for subduction-related rocks (blue shaded field) highlight the non–steady-state record of magmatism during construction of Zealandia and the Median Batholith. Data are not standardized to area; see Figure 9 for areal addition rate plot for Fiordland. SPS—Separation Point Suite granitic rocks; WFO—Western Fiordland Orthogneiss.**

TABLE 1. SAMPLE LOCALITIES AND GEOCHRONOLOGY SUMMARY

| Sample | P Collection | Pluton | Rock type* | Location | Lat (°S) | Long | Age (Ma; 2σ standard error) | MSWD | Number of zircons† |
|---|---|---|---|---|---|---|---|---|---|
| 5NZ12 | P85714 | Eastern McKerr intrusives | Two-mica granite | George Sound | 44.965201 | 167.426942 | 128.3 ± 3.9 | 1.6 | 4 |
| 15NZ20 | P85715 | Eastern McKerr intrusives | Hbl diorite | George Sound | 44.899746 | 167.387870 | 120.1 ± 2.8 | 1.6 | 9 |
| 12NZ17B | P83645 | Malaspina Pluton | Grt-bearing leucosome | Breaksea Sound | 45.568569 | 166.793545 | 117.0 ± 1.0 | 0.4 | 11 |
| 13NZ16B | P83712 | Malaspina Pluton | Hbl diorite | Acheron Passage | 45.693742 | 166.720344 | 118.0 ± 2.1 | 1.4 | 10 |
| 13NZ22 | P83718 | Malaspina Pluton | Hbl diorite | Breaksea Sound | 45.569681 | 166.790631 | 116.9 ± 1.6 | 0.3 | 8 |
| 13NZ34A | P83730 | Malaspina Pluton | Two-pyroxene diorite | Acheron Passage | 45.654666 | 166.718933 | 118.0 ± 1.8 | 1.4 | 8 |
| 13NZ40D-1 | P83733 | Malaspina Pluton | Bt-Hbl diorite with relict pyroxene | Vancouver Arm | 45.549658 | 166.853386 | 116.4 ± 1.3 | 1.0 | 8 |
| 13NZ59 | P83750 | Malaspina Pluton | Hbl-Bt Qz diorite | First Arm | 45.340134 | 166.912906 | 117.5 ± 1.0 | 2.0 | 7 |
| 12NZ22A | P83650 | Misty Pluton | Hbl diorite | South of Gaer Arm | 45.307248 | 167.109253 | 114.7 ± 1.1 | 0.2 | 12 |
| 12NZ24 | P83652 | Misty Pluton | Hbl diorite | Marrington Peaks | 45.344945 | 167.172045 | 115.8 ± 2.1 | 1.5 | 8 |
| 12NZ33 | P83661 | Misty Pluton | Hbl monzodiorite | Bradshaw Sound | 45.305890 | 167.153981 | 114.3 ± 2.1 | 2.6 | 8 |
| 12NZ36B | P83664 | Misty Pluton | Bt-Hbl Qz diorite with relict pyroxene | Bradshaw Sound | 45.271430 | 167.138984 | Pop 1: 114.2 ± 1.3 | 0.4 | 2 |
| 12NZ36B | P83664 | Misty Pluton | Bt-Hbl Qz diorite with relict pyroxene | Bradshaw Sound | 45.271430 | 167.138984 | Pop 2: 119.7 ± 1.3 | 0.4 | 7 |
| 12NZ36B | P83664 | Misty Pluton | Bt-Hbl Qz diorite with relict pyroxene | Bradshaw Sound | 45.271430 | 167.138984 | Pop 3: 127.9 ± 1.2 | 1.1 | 7 |
| 13NZ46 | P83738 | Misty Pluton | Two-pyroxene monzodiorite | Caswell Sound | 45.044192 | 167.290175 | 116.9 ± 1.2 | 0.6 | 12 |
| 13NZ52A | P83743 | Misty Pluton | Two-pyroxene diorite | Charles Sound | 45.092523 | 167.156780 | 116.8 ± 1.6 | 1.1 | 9 |
| 13NZ55A | P83746 | Misty Pluton | Hbl-Bt Qz diorite | Nancy Sound | 45.114086 | 167.039648 | 115.2 ± 1.9 | 1.3 | 10 |
| 13NZ58 | P83749 | Misty Pluton | Two-pyroxene diorite | Nancy Sound | 45.155586 | 167.090876 | 115.3 ± 1.5 | 0.5 | 8 |
| 14NZ34A | P83848 | Western McKerr intrusives | Bt-Hbl diorite | Caswell Sound | 45.020713 | 167.214870 | 118.4 ± 0.9 | 0.4 | 8 |
| 14NZ35A | P83849 | Western McKerr intrusives | Hbl diorite | Caswell Sound | 45.012009 | 167.194568 | 117.7 ± 1.6 | 2.1 | 8 |
| 15NZ2 | P85716 | Worsley Pluton | Two-pyroxene diorite | Bligh Sound | 44.871556 | 167.522328 | 121.6 ± 1.9 | 0.7 | 10 |
| 15NZ27 | P85717 | Worsley Pluton | Two-pyroxene diorite | Bligh Sound | 44.780061 | 167.517868 | 123.2 ± 1.6 | 1.0 | 13 |

*Note:* P Collection— sample identification number in the GNS Petlab collection (http://pet.gns.cri.nz/#/); MSWD—mean square of weighted deviates. Pop—population.
*Mineral abbreviations after Whitney and Evans (2010).
†Zircons used in age calculations.

TABLE 2. AREAL ADDITION RATES FOR THE MEDIAN BATHOLITH (INCLUDING WESTERN FIORDLAND ORTHOGNEISS)

| Intrusive suite | Area ($km^2$) | Assumed paleothickness (km)* | Crystallization age/age range (Ma) | Duration of magmatism (m.y.)† | Areal addition rate ($km^2$/ m.y.) | Magma addition rate ($km^3$/m.y.) | References§ |
|---|---|---|---|---|---|---|---|
| **Separation Point Suite; WFO component in western Fiordland (lower crust; *P* > 10 kbar)** | | | | | | | |
| Worsley | 569.0 | 25 | 124–121.8 | 2.2 | 259 | 6466 | 1, 2, 3, 4 |
| McKerr East | 155.1 | 25 | 120.1–128.3 | 8.2 | 19 | 473 | 1, 4 |
| McKerr West | 72.6 | 25 | 118.4–117.7 | 1.0 | 73 | 1816 | 1, 8 |
| Misty | 669.7 | 25 | 116.8–114.2 | 2.5 | 268 | 6697 | 1, 9 |
| Malaspina | 554.0 | 25 | 118.0–115.4 | 2.6 | 213 | 5327 | 1, 2, 4, 5, 6 |
| Northwest Malaspina | 54.6 | 25 | 117.5 ± 1.0 | 2.0 | 27 | 683 | 1 |
| Breaksea Orthogneiss | 46.7 | 25 | 123.2 ± 1.3 | 2.6 | 18 | 449 | 7 |
| Resolution Island Orthogneiss | 25.2 | 25 | 115.1 ± 1.6 | 3.2 | 8 | 197 | 6 |
| Omaki Orthogneiss | 39.6 | 25 | 127.9–124.9 | 3.0 | 13 | 330 | 12 |
| Supper Cove Orthogneiss | 135.3 | 25 | 128 ± 1 | 2.0 | 68 | 1691 | 2 |
| Mount Edgar Diorite | 25.8 | 25 | 128.8 ± 2.4 | 4.8 | 5 | 134 | 5 |
| Total Lower Crust | 4461.0 | | | | | | |
| **SPS WFO/Host Rock (%)** | **52.6** | | | | | | |
| **Separation Point Suite TTG component in eastern Fiordland (middle crust; *P* = 4–9 kbar)** | | | | | | | |
| Refrigerator Orthogneiss | 118.0 | 25 | 120.7 ± 1.1 | 2.2 | 54 | 1341 | 10 |
| Puteketeke Pluton | 164.7 | 25 | 120.8–119.9 | 1.0 | 165 | 4117 | 10, 12 |
| West Arm Leucogranite | 259.8 | 25 | 116.3 ± 1.2 | 2.4 | 108 | 2707 | 10 |
| North Fiord Granite (upper crust) | 35.2 | 25 | 122.0 ± 1.7 | 3.4 | 10 | 259 | 3 |
| Takahe Granodiorite | 0.1 | 25 | 122.4 ± 2.2 | 4.4 | 0 | 0 | 3 |
| Titiroa Granite | 100.8 | 25 | 122.5 ± 1.9 | 3.8 | 27 | 663 | 3 |
| Caroline Pluton | 15.0 | 25 | n.d. | n.d. | n.d. | n.d. | n.d. |
| Mount George Gabbro | 48.4 | 25 | 127 | n.d. | n.d. | n.d. | 17 |
| Indecision Creek Complex | 111.4 | 25 | 135–124 | 11.0 | 10 | 253 | 17 |
| Total Middle crust | 3743.0 | | | | | | |
| **SPS TTG/Host Rock (%)** | **22.8** | | | | | | |

(*continued*)

TABLE 2. AREAL ADDITION RATES FOR THE MEDIAN BATHOLITH (INCLUDING WESTERN FIORDLAND ORTHOGNEISS) (*continued*)

| Intrusive suite | Area ($km^2$) | Assumed paleothickness (km)* | Crystallization age/age range (Ma) | Duration of magmatism (m.y.)† | Areal addition rate ($km^2$/ m.y.) | Magma addition rate ($km^3$/m.y.) | References§ |
|---|---|---|---|---|---|---|---|
| **Separation Point Suite TTG component in southwest Fiordland (upper crust; *P* < 4 kbar)** | | | | | | | |
| Spot 59 Pluton | 17.6 | 5 | 115–105 | 10.0 | 2 | 9 | 18 |
| Prices Pluton | 3.0 | 5 | 115–105 | 10.0 | 0 | 2 | 18 |
| Five Fingers Pluton | 21.3 | 5 | 118.4 ± 0.7 | 1.4 | 15 | 76 | 12 |
| Mouat Pluton | 32.9 | 5 | 125–115 | 10.0 | 3 | 16 | 18 |
| Only Islands Diorite | 6.1 | 5 | 122 ± 1 | 2.0 | 3 | 15 | 20 |
| Bald Peaks Pluton | 6.9 | 5 | 122 | n.d. | n.d. | n.d. | 12 |
| Fannin Pluton | 22.9 | 5 | 121 ± 33 | 66.0 | 0 | 2 | 12 |
| Anchor Island Intrusives #3 | n.d. | 5 | 115-105 | 10.0 | n.d. | n.d. | 18 |
| Total Upper Crust | 3022.0 | | | | | | |
| **SPS TTG/Host Rock (%)** | **3.7** | | | | | | |
| **Rahu Suite in southwest Fiordland (shallow crust; *P* < 4 kbar)** | | | | | | | |
| Brothers Pluton | 123.1 | 5 | 120.8 ± 0.1 | 1.0 | 123 | 615 | 12 |
| Treble Mountain Pluton | 17.1 | 5 | 130.0–127.5 | 2.5 | 7 | 34 | 12, 20 |
| Red Head Pluton | 4.6 | 5 | 121.1 ± 0.2 | 1.0 | 5 | 23 | 12 |
| North Port granite | 12.1 | 5 | 128.7 ± 0.3 | 1.0 | 12 | 61 | 12 |
| Lake Monk Granite | 11.0 | 5 | 135 ± 6 | 12.0 | 1 | 5 | 12? |
| Revolver Pluton | 116.6 | 5 | 130.9 ± 0.15 | 1.0 | 117 | 583 | 20 |
| Indian Island Granite | 41.2 | 5 | 126 | n.d. | n.d. | n.d. | 12 |
| Trevaccoon Pluton | 6.1 | 5 | 129 ± 1.0 | 2.0 | 3 | 15 | 20 |
| Anchor Island Intrusives #2 | n.d. | 5 | 115 ± 1.7 | 3.4 | n.d. | n.d. | 12 |
| Total Upper Crust | 3022.0 | | | | | | |
| **Rahu TTG/Host Rock (%)** | **11.0** | | | | | | |
| **SPS and Rahu/Host Rock (%)** | **14.6** | | | | | | |
| **Darran Suite (undivided, mostly middle crust)** | | | | | | | |
| Middle Poteriteri Pluton | 6.1 | 25 | 125 ± 10 | 20.0 | 0 | 8 | 18 |
| Murchison Intrusives | 120.9 | 25 | 137.1 ± 0.1 | 1.0 | 121 | 3022 | 12 |
| Largs Group | 21.5 | 5 | 140 ± 2 | 4.0 | 5 | 27 | 19 |
| Darran Leucogabbro | 316.0 | 25 | 141–135 | 6.0 | 53 | 1317 | 11 |
| Nurse Suite | 34.8 | 25 | 141–140.8 | 1.0 | 35 | 870 | 8, 10 |
| Glade Suite | 21.1 | 25 | 142–140.6 | 1.4 | 15 | 376 | 8, 10 |
| Halfway Peak Hornblende Gabbro | 33.0 | 25 | 146.0 ± 2.2 | 4.4 | 8 | 188 | 11 |
| Harrison Gneiss | 35.3 | 25 | 146.5–146.2 | 1.0 | 35 | 882 | 16 |
| Cleughearn Pluton | 26.6 | 25 | 154.5-153.8 | 1.4 | 19 | 475 | 13 |
| Mount Luxmore Mafic Complex | 15.9 | 25 | 158.8 ± 2.3 | 4.6 | 3 | 87 | 13 |
| Hunter Intrusives | 240.8 | 25 | 170–130 | 40.0 | 6 | 151 | 10, 11, 13, 15 |
| Howitt Peaks Gabbro | 6.2 | 25 | 170–130 | 40.0 | 0 | 4 | 17 |
| Hanging Valley Granitoid Intrusives | 5.4 | 25 | 170–130 | 40.0 | 0 | 3 | 17 |
| Dana tonalite | 5.3 | 25 | 170–130 | 40.0 | 0 | 3 | 17 |
| West Kepler Gabbro | 8.7 | 25 | 175–140 | 35.0 | 0 | 6 | 17 |
| Selwyn Creek Gneiss | 15.8 | 25 | 176.9–154.4 | 22.5 | 1 | 18 | 5, 16 |
| Loch Burn Formation | 33.3 | 5 | 195–145 | 40.0 | 1 | 4 | 11, 15 |
| Mistake Suite | 70.8 | 25 | 224 ± 6 | 12.0 | 6 | 148 | 11 |
| Holly Burn Intrusives | 112.5 | 25 | 232 ± 3 | 6.0 | 19 | 469 | 21 |
| Hut Leucogranite | 10.5 | 25 | n.d. | n.d. | n.d. | n.d. | 17 |
| Mount Anau Complex | 2.7 | 25 | n.d. | n.d. | n.d. | n.d. | n.d. |

*Note*: WFO—Western Fiordland Orthogneiss; SPS—Separation Point Suite; *P*—pressure; TTG—tonalite-trondhjemite-granodiorite; n.d.—no data.

*Pluton thicknesses assumed to be 25 km for lower and middle crust, and 5 km for shallow crust. Volcanic assemblages are assigned 5 km thicknesses.

†Durations calculated as follows. For plutons with single dates, durations are based on assigned 2σ weighted average errors. For high precision thermal ionization mass spectrometry dates, pluton construction is assumed to occur over at least ~1 m.y. (cf. Coleman et al., 2004). For cases where there are multiple dates, durations are calculated as the difference between oldest and youngest dates.

§References: 1—this study; 2—Tulloch and Kimbrough (2003); 3—Bolhar et al. (2008); 4—Hollis et al. (2004); 5—Hollis et al. (2003); 6—Klepeis et al. (2016); 7—Hout et al. (2012); 8—Klepeis et al. (2004); 9—Allibone et al. (2009b); 10—Scott and Palin (2008); 11—Kimbrough et al. (1994), 12—Ramezani and Tulloch (2009); 13—Muir et al. (1998); 14—Marcotte et al. (2005); 15—Scott et al. (2008); 16—Decker (2016); 17—undated (date estimated in Allibone et al., 2009a); 18—undated (date estimated in Allibone et al., 2007); 19—Mortimer et al. (1999); 20—Gollan et al. (2005); 21—McCoy-West et al. (2014).

is not confirmed (e.g., Tulloch and Kimbrough, 2003; Allibone et al., 2009a, 2009b).

Plutonic rocks of the Darran Suite are composed of a bimodal suite of mafic and felsic, low Sr/Y (<40) gabbro, diorite, quartz diorite, quartz monzodiorite, tonalite, granodiorite, and monzogranite. Muir et al. (1998) observed that outboard Darran Suite rocks show enrichments in large ion lithophile elements (e.g., Rb, Ba, Th, K) and light rare earth elements (REEs), and depletions in mantle-normalized Nb values, consistent with derivation from a subduction zone setting. Radiogenic isotopes values are primitive; initial $^{87}Sr/^{86}Sr$ ratios range from 0.7037 to 0.7049, and initial $\varepsilon_{Nd}$ values cluster at +3 to +4 (Muir et al., 1998). These features together with the lack of observed zircon inheritance suggest that outboard Darran Suite magmas underwent little to no interaction with preexisting continental crust during their petrogenesis.

### *Separation Point Suite*

The Separation Point Suite consists of a suite of high-Sr/Y (>40) plutonic rocks emplaced between ca. 128 and 105 Ma (Tulloch and Kimbrough, 2003). Felsic plutonic rocks include tonalites, trondhjemites, granodiorites, and granites that form two major belts in Fiordland and Nelson-Westland (northwestern South Island). The Separation Point Suite belts are currently divided into two sections by the Alpine fault. In the Nelson-Westland area, the Separation Point Suite includes elongate intrusive bodies that strike northeast–southwest for ~120 km (Muir et al., 1995; Bolhar et al., 2008; Sagar et al., 2016). In eastern Fiordland, they comprise a north-south–trending elongate plutonic complex (e.g., Muir et al., 1998; Bolhar et al., 2008; Scott and Palin, 2008; Allibone et al., 2009a). A minor volume of this component occurs in upper crustal rocks in southwestern Fiordland as small intrusive bodies along the Tasman Sea (Fig. 2). The Separation Point Suite plutonic belt is mostly inboard of the Darran Suite plutonic belt, but intrusions into the outboard Darran Suite are also common (Tulloch and Kimbrough, 2003). Ages for the Separation Point Suite in Westland-Nelson range from 127 to 112 Ma (Muir et al., 1995; Bolhar et al., 2008; Sagar et al., 2016), in eastern Fiordland ages range from 123 to 116 Ma (Bolhar et al., 2008; Scott and Palin, 2008; Ramezani and Tulloch, 2009), and in southwestern Fiordland ages range from 122 to 118 Ma (Ramezani and Tulloch, 2009). On Stewart Island, dates range from 128 to 105 Ma (Allibone and Tulloch, 2004). The relative locations of older Darran Suite and younger Separation Point Suite plutonic belts clearly record progressively younger arc activity migrating inboard from ca. 230 Ma to ca. 100 Ma. Emplacement pressures for the Darran and Separation Point Suite rocks range from 2 to 7 kbar (Tulloch and Challis, 2000; Allibone and Tulloch, 2008; Scott et al., 2009).

Mafic plutonic rocks of the Separation Point Suite are the focus of this study and include seven variably metamorphosed Early Cretaceous plutons of the Western Fiordland Orthogneiss. It occupies >2300 $km^2$ and consists of diorite, quartz diorite, monzodiorite, and minor gabbro (Fig. 3). Allibone et al. (2009b) distinguished plutons based on emplacement ages, petrography, structural and metamorphic features, and geochemistry (see Allibone et al., 2009b, for a detailed description of the plutons). Plutons of the Western Fiordland Orthogneiss in Fiordland that were sampled in this study include the Worsley, Misty, and Malaspina Plutons, and the eastern and western McKerr Intrusives (Fig. 3). The Western Fiordland Orthogneiss is estimated to have been emplaced at 10–18 kbar (see Allibone et al., 2009b, and references therein), synchronous with regional transpression/contractional deformation in northern Fiordland, in Caswell Sound in western Fiordland (Daczko et al., 2001, 2002; Klepeis et al., 2004; Marcotte et al., 2005), in the Grebe mylonite zone in eastern Fiordland (Scott et al., 2011), and the Freshwater fault system, Escarpment fault, and Gutter shear zone on Stewart Island (Allibone and Tulloch, 2008).

## METHODS

### U-Pb Zircon Geochronology and Trace Element Methods

Zircons were separated using standard mineral separation procedures involving crushing, density separation on a Wilfley water table, magnetic separation up to 1.5A using a Frantz isodynamic separator, and methylene iodide heavy liquid. Approximately 50–80 zircons were picked from each sample using a Leica S8APO binocular microscope for casting in epoxy. Zircons were selected on the basis of being clear, colorless, and inclusion free. Some samples had bimodal grain sizes, and thus the suites of zircons were picked to represent each size fraction. Cathodoluminescence (CL) images were collected using a FEI Quanta 600 scanning electron microscope (SEM) at the California State University Northridge scanning electron microscope laboratory for the purpose of detecting internal structures, inclusions, and physical defects of the zircons (Fig. 5). U-Pb zircon geochronology and trace element analyses were conducted at the Stanford–U.S. Geological Survey SHRIMP-RG facility. Detailed descriptions of methods for isotopic analysis are given in the Data Repository Item[1], and summarized in Table 1. All zircon CL images, ion probe spot locations, and chondrite-normalized REE patterns are also provided in the Data Repository Item.

### Zircon Thermometry

We use SHRIMP-RG measurements of Ti concentrations collected simultaneously with $^{206}Pb/^{238}U$ isotopic ages, and the Ferry and Watson (2007) calibration to calculate temperatures associated with zircon growth (Fig. 5). All samples contain quartz fixing the $aSiO_2$ at unity. Several samples with granulite facies mineral assemblages contain rutile; however, samples that retain original igneous mineral assemblages generally lack rutile, suggesting that rutile is likely a secondary metamorphic phase. We therefore present model Ti-in-zircon temperatures calculated assuming an absence of rutile and estimate the activity of $TiO_2$ at 0.6 based on the presence of ilmenite. In cases where rutile was part of the igneous assemblage, our corrected Ti-in-zircon temperatures would overestimate crystallization temperatures by ~50 °C. Both calculations are presented in the Data Repository data trace element zircon data file.

### Areal and Magma Addition Rate Calculations

U-Pb zircon dates are used to determine time scales of magmatism and establish links between periods of high magma flux and tectonic events. We calculate both areal intrusive rates ($km^2$/m.y.) and magma addition rates ($km^3$/m.y.) from zircon crystallization ages and area estimates modified from GNS QMAP geographic information system data (Turnbull et al., 2010). Estimation of magmatic fluxes follows the strategy outlined by Gehrels et al. (2009) and involves (1) subdividing the Median Batholith into shallow, middle, and lower crustal components based on emplacement pressures where known, (2) subdividing plutonic units into temporally homogeneous segments, (3) subtracting nonplutonic rocks from area estimates, (4) multiplying the area of exposed lower and middle crustal plutonic rocks by a thickness of 25 km, and shallow plutonic rocks by a thickness of 5 km (for MAR calculations), and (5) dividing the resulting value by the duration of magmatism in each region to determine average

[1]GSA Data Repository Item 2017080, Zircon rare earth element plots, cathodoluminescence images, sample location information, and zircon isotope and geochemical data, is available at www.geosociety.org/datarepository/2017, or on request from editing@geosociety.org.

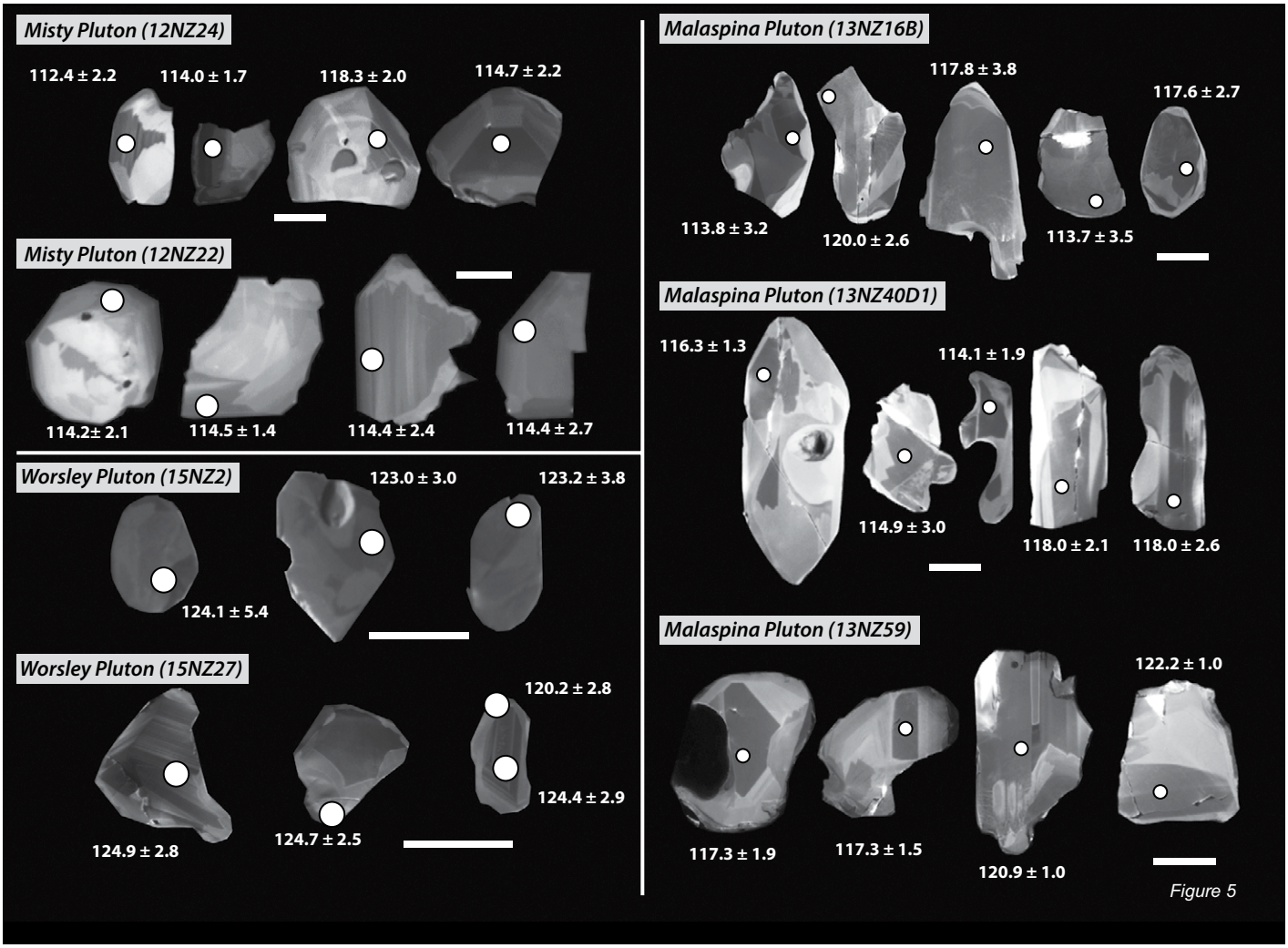


**Figure 5. Cathodoluminescence images of representative zircons from the Western Fiordland Orthogneiss. Solid white circles indicate location of sensitive high-resolution ion microprobe–reverse geometry (SHRIMP-RG) spots where U-Pb isotopes and trace element concentrations were collected simultaneously. Quoted uncertainties are 1σ. Scale bars are 100 μm.**

magmatic fluxes. Emplacement depths are assigned as follows: shallow crust is represented by southwestern Fiordland, where emplacement pressures are ≤4 kbar; middle crustal depths are observed in eastern Fiordland, where emplacement pressures are 4–9 kbar; and lower crustal depths are observed in western Fiordland, where pressures are >10 kbar (Tulloch and Challis, 2000; Allibone et al., 2007, 2009a, 2009b, 2009c; Scott et al., 2009). Durations of magmatism are difficult to quantify because some plutons are undated, some have a single date, and some have multiple dates. For plutons with single dates, we calculate durations based on assigned 2σ weighted average errors. For cases where there are multiple dates, durations are calculated as the difference between oldest and youngest dates. In the case of high-precision thermal ionization mass spectrometry (TIMS) dates with 2σ errors <1 m.y., we assume a minimum time scale of at least 1 m.y. for pluton construction (e.g., Coleman et al., 2004). The choice of 25 km pluton thicknesses for MAR calculations for the lower crustal Western Fiordland Orthogneiss is assumed as a lower limit based on seismic velocity data beneath the orthogneiss that indicates that mafic and/or ultramafic arc crust extends to depths of 40 km (Eberhart-Phillips and Reyners, 2001). The use of 25 km for lower and middle crustal also allows direct comparison to published values in other well-studied orogenic belts (e.g., Coast Mountains Batholith, Sierra Nevada Batholith, North Cascades plutonic complex: Ducea and Barton, 2007; Gehrels et al., 2009; Paterson et al., 2011). We note that the precise amount of the high-velocity root that is Western Fiordland Orthogneiss is uncertain and some component is likely ultramafic cumulate or underplated material; we therefore emphasize and show areal addition calculations, but present both in Table 2.

## RESULTS

### Sample Descriptions

Samples were collected (using helicopter and boat) from ~3000 km$^2$ of lower crust in western Fiordland. Our data span ~130 km parallel and ~30 km perpendicular to the strike of the paleoarc axis, which is roughly approximated by the present-day western Fiordland coastline (Figs. 2 and 3). Sampling includes (from north to south) two samples of the Worsley Pluton, two samples from the eastern McKerr Intrusives,

two samples from the western McKerr Intrusives, eight samples from the Misty Pluton, and six samples from the Malaspina Pluton. Locations are shown in Figure 3 and Table 1. The geology of major Western Fiordland Orthogneiss plutons was given in Allibone et al. (2009b). For deformation and metamorphic descriptions of the Western Fiordland Orthogneiss, see Oliver (1976, 1977), Bradshaw (1989c, 1990), Gibson and Ireland (1995), Clarke et al. (2000), Daczko et al. (2002), Hollis et al. (2004), Klepeis et al. (2004, 2007, 2016), Allibone et al. (2009b), De Paoli et al. (2009), and Stowell et al. (2014).

### Internal Zircon Textures in CL

Zircons from the Western Fiordland Orthogneiss are characterized by weak oscillatory zoning and irregular external appearances, consistent with late-stage igneous zircon growth from a mafic magma and/or very slow and complex crystallization during prolonged residence in the lower crust (Fig. 5) (Corfu et al., 2003). Sector zoning is also common. Some zircons display embayment and truncation of growth zoning suggesting resorption during granulite to amphibolite facies metamorphism (Clarke et al., 2000; Stowell et al., 2014; Schwartz et al., 2016). In some cases, 1–5 µm luminescent, metamorphic rims overgrow weak oscillatory zoning textures; however, these domains were generally avoided during SHRIMP-RG analyses.

### Zircon Geochronology

#### *Malaspina Pluton*

The Malaspina Pluton spans >500 km$^2$ and consists of diorite, hornblende diorite, and monzodiorite with scarce hornblendite and garnet pyroxenite (Oliver, 1976, 1980; Allibone et al., 2009b). Our sampling consists of two diorites from Acheron Passage south of Breaksea Sound, a hornblende diorite and a garnet-bearing trondhjemite vein from John Island in Breaksea Sound, a diorite from Vancouver Arm, and a hornblende diorite from First Arm.

A hornblende diorite (13NZ59) from First Arm yielded eight individual SHRIMP-RG spot analyses from eight individual zircon grains that are concordant and yield dates ranging from 122.2 ± 1.0 Ma to 117.3 ± 1.9 Ma. One spot analysis yielded a statistically younger age (113.1 ± 2.6 Ma) than the majority of the population and could be a product of new metamorphic growth during granulite facies metamorphism (Stowell et al., 2014; Schwartz et al., 2016); therefore it was excluded from the error-weighted average calculation. The remaining seven zircons yielded an error-weighted average $^{206}Pb/^{238}U$ age of 120.3 ± 1.8 Ma (mean square of weighted deviates, MSWD = 2.0; Fig. 6A). The slightly high MSWD (2.0) may indicate mixing of two components, although CL images do not reveal obvious xenocrysts (Fig. 5). Using Isoplot 3.75 (Ludwig, 2012), which includes a partial implementation of the Sambridge and Compston (1994) mixture modeling method for deconvolution of suites of zircons that have multiple age components, the complex range of zircon dates was separated into 2 populations which yield ages of 117.5 ± 1.0 Ma (relative percentage = 43%), 121.3 ± 0.6 Ma (relative percentage = 57%) with a relative misfit of 0.43. In this case, the 117.5 Ma age corresponds to the timing of magmatic emplacement and the 121.3 Ma component represents older zircon xenocrysts. In the absence of additional information, we view both age interpretations as viable. These results overlap with several existing ages from Doubtful Sound including two SHRIMP ages of 115.9 ± 1.2 Ma (Klepeis et al., 2016) and 115.6 ± 2.4 Ma (Hollis et al., 2004), and three laser ablation–multicollector–inductively coupled plasma–mass spectrometry (LA-MC-ICP-MS) ages of 114.2 ± 1.6 Ma, 115.4 ± 1.7 Ma, and 116.1 ± 1.7 Ma (Stowell et al., 2014).

A two-pyroxene diorite sample (13NZ34A) from Acheron Passage yielded eight concordant individual SHRIMP-RG spot analyses from eight individual zircon grains. Analyses range from 114.9 ± 2.4 Ma to 120.4 ± 1.0 Ma and yield an error-weighted average $^{206}Pb/^{238}U$ age of 118.0 ± 1.8 Ma (MSWD = 1.4; Fig. 6B). Another sample from Acheron Passage, a hornblende diorite (sample 13NZ16B), yielded 10 individual SHRIMP-RG spot analyses from 10 individual zircon grains (Fig. 5). These analyses yielded dates ranging from 112.0 ± 2.7 Ma to 120.5 ± 1.1 Ma. The error-weighted average $^{206}Pb/^{238}U$ age of all 10 zircons is 118.0 ± 2.1 Ma (MSWD = 1.4; Fig. 6D). An existing U-Pb zircon TIMS date ~20 km to the east in Wet Jacket Arm yielded an age of 116.6 ± 1.2 Ma, which overlaps our results within uncertainty (Mattinson et al., 1986; Tulloch and Kimbrough, 2003).

The biotite hornblende diorite with relict pyroxene sample from Breaksea Sound on Vancouver Arm (sample 13NZ40D1) yielded nine concordant individual SHRIMP-RG spot analyses from nine separate zircons with dates that range from 112.6 ± 2.5 to 119.9 ± 1.9 Ma. One individual zircon analysis yielded a much younger date of 107.4 ± 3.4 Ma. This date could be a product of new metamorphic growth because it overlaps metamorphic zircon dates from granulite facies marbles in the Doubtful Sound shear zone in First Arm, which give a metamorphic zircon age of 105.6 ± 1.9 Ma (Schwartz et al., 2016). This suggestion is consistent with the highly rounded and embayed morphology of zircons from this sample, which likely underwent some dissolution during metamorphism (Fig. 5). The remaining zircons give an error-weighted average $^{206}Pb/^{238}U$ age of 116.4 ± 1.3 Ma (MSWD = 1.0; Fig. 6C). Another deformed hornblende diorite near Breaksea Sound (sample 13NZ22) yielded eight separate, concordant SHRIMP-RG spot analyses from eight individual zircon grains that range from 114.2 ± 3.0 Ma to 118.5 ± 2.8 Ma. The error-weighted average $^{206}Pb/^{238}U$ age of all spots is 116.9 ± 1.6 Ma (MSWD = 0.31; Fig. 6E).

***Garnet-Bearing vein.*** A garnet-bearing trondhjemite vein (12NZ17B) that crosscuts host diorite near 13NZ22 (above) yielded 11 individual SHRIMP-RG spot analyses from 11 individual zircon grains ranging from 114.0 ± 2.5 Ma to 119.0 ± 2.9 Ma. The error-weighted average $^{206}Pb/^{238}U$ age is 117.0 ± 1.0 Ma (MSWD = 0.35; Fig. 6F), statistically indistinguishable from the error-weighted average age of the host. One spot analysis produced a relatively older age (121.5 ± 0.8 Ma) suggesting that it might be a xenocryst; it was excluded from the error-weighted average $^{206}Pb/^{238}U$ age calculation.

#### *Misty Pluton*

The Misty Pluton occupies >670 km$^2$ and is the largest unit in the Western Fiordland Orthogneiss. Allibone et al. (2009b) distinguished three magmatic phases that include (1) a pale, medium-grained, two-pyroxene ± hornblende diorite and monzodiorite in the northern and central portions of the Misty Pluton; (2) a darker, medium- to coarse-grained diorite and quartz monzodiorite with relict corroded clinopyroxene in the southern portion of the pluton around Doubtful Sound; and (3) a dark, medium-grained, commonly strongly foliated hornblende-rich diorite located along the eastern margin of the pluton. Our sampling consists of two samples from the two-pyroxene diorite phase, three samples from the hornblende diorite with the relict pyroxene phase, and three samples from the hornblende-rich phase.

***Two-Pyroxene Diorite Phase.*** One sample from Caswell Sound (13NZ46) yielded 12 individual SHRIMP-RG analyses from 12 separate zircon grains. The majority of $^{206}Pb/^{238}U$ dates range from 113.0 ± 3.0 Ma to 119.2 ± 1.5 Ma. One zircon has an older age of 123.6 ± 1.7 Ma, and is likely a xenocryst. Excluding this older analysis, the error-weighted averaged $^{206}Pb/^{238}U$ age is 116.9 ± 1.2 Ma (MSWD = 0.64; Fig. 6G). Another two-pyroxene monzonite from Emileus Arm in Charles Sound (sample 13NZ52A) yielded nine individual SHRIMP-RG spot analyses

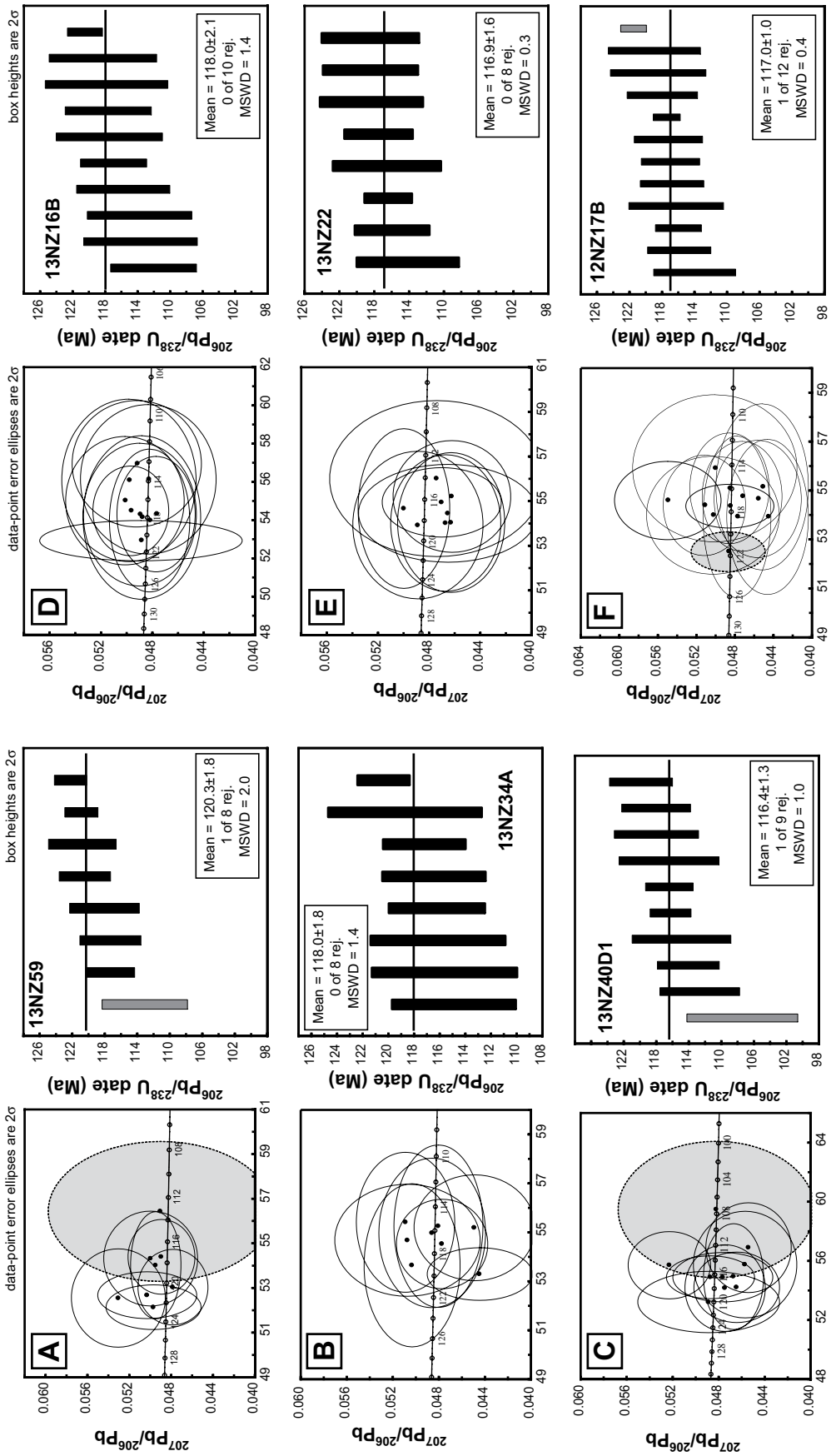


**Figure 6. Zircon Tera-Wasserburg concordia diagrams and weighted average age plots. Concordia and weighted average diagrams show all analyzed spots (including rejected [rej.] spots in gray). Error ellipses show 2σ total uncertainty for individual spot analyses. MSWD—mean square of weighted deviates. (*Continued on following two pages.*)**

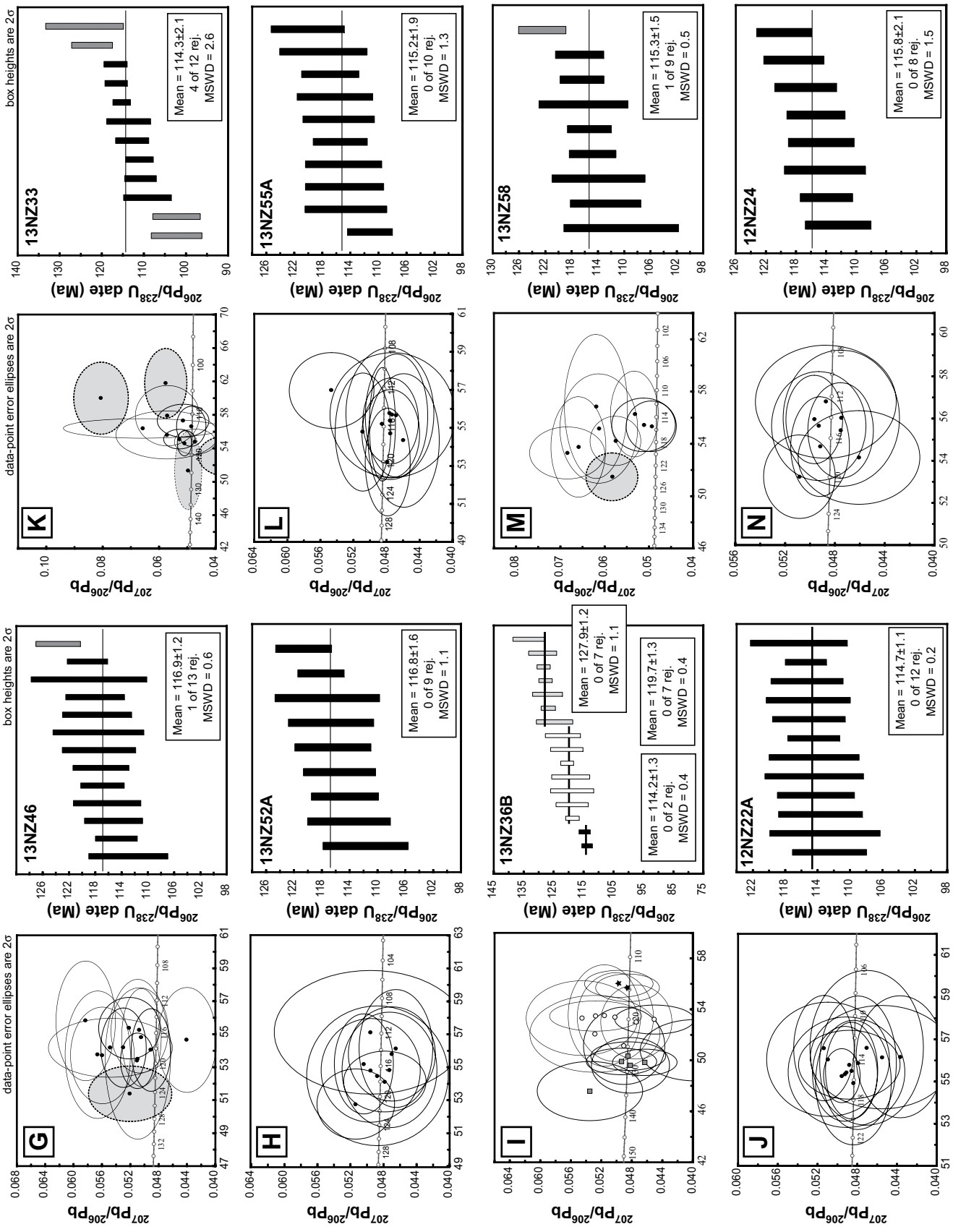


**Figure 6 (*continued*).**

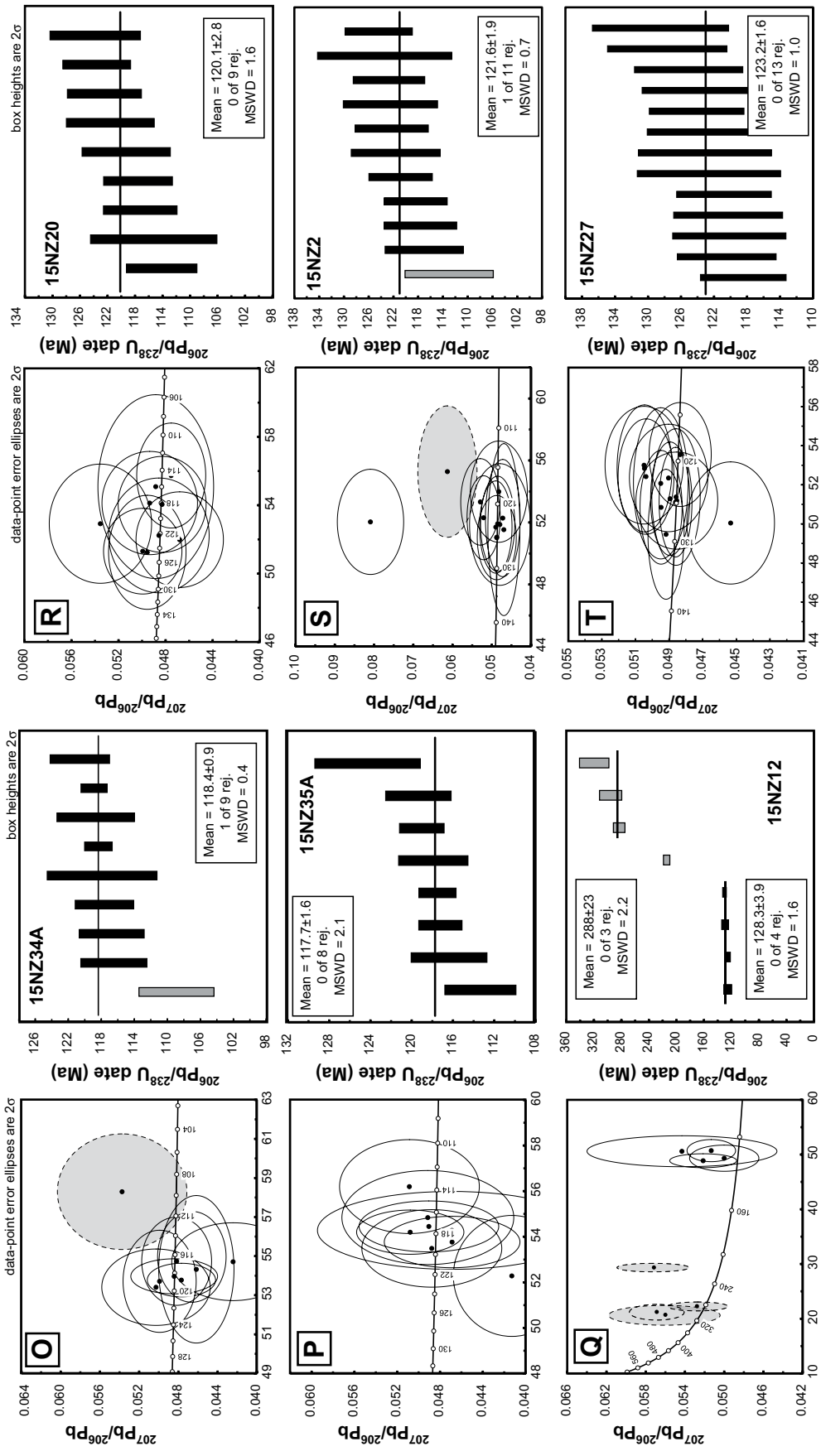


**Figure 6 (*continued*).**

from nine individual zircon grains ranging from 111.7 ± 3.1 Ma to 120.6 ± 2.0 Ma. The error-weighted average $^{206}Pb/^{238}U$ age is 116.8 ± 1.6 Ma (MSWD = 1.11; Fig. 6H).

***Relict Pyroxene Diorite Phase.*** The most complex and unique sample is a biotite hornblende quartz diorite from McDonnell Island in Bradshaw Sound (sample 12NZ36B). Individual zircon spot analyses (n = 16) from 16 individual grains yielded an overdispersion in dates from 106 ± 12 to 133 ± 3 Ma (Fig. 6I). The error-weighted average $^{206}Pb/^{238}U$ age of all zircons is 121.2 ± 3.2 Ma (MSWD = 17). One zircon $^{206}Pb/^{238}U$ age was omitted from the calculations because it has a much younger age and large uncertainty (105.8 ± 12.1 Ma). The young age could represent new metamorphic growth during metamorphism, because it correlates with $^{206}Pb/^{238}U$ metamorphic zircon ages in the Doubtful Sound shear zone (105.6 ± 1.9 Ma; Schwartz et al., 2016). The large MSWD value for the sample population indicates scatter in excess of the analytical error. Deconvolution using the Sambridge and Compston (1994) mixture modeling method yields ages of 114.2 ± 0.7 Ma (relative percentage = 13%), 119.8 ± 0.7 Ma (relative percentage = 44%), and 127.9 ± 0.6 Ma (relative percentage = 44%) with a relative misfit of 0.089. In this case, the older 127.9 Ma population likely represents xenocrystic cargo, whereas the youngest 114.2 Ma population may represent either the latest magmatic phase or recrystallization during granulite facies metamorphism. In the absence of additional information, it is possible that either the 114.2 or the 119.8 Ma populations may be magmatic.

A biotite hornblende monzodiorite with relict pyroxene from Bradshaw Sound (sample 12NZ22A) yielded 12 individual SHRIMP-RG spot analyses on 12 separate zircon grains with a $^{206}Pb/^{238}U$ date range of 112.5 ± 2.0–116.3 ± 2.6 Ma (Fig. 5). The error-weighted average $^{206}Pb/^{238}U$ age of all the zircons is 114.7 ± 1.1 Ma (MSWD = 0.19; Fig. 6J). Another sample from Bradshaw Sound, a hornblende monzodiorite with relict pyroxene (sample 12NZ33), yielded 12 separate SHRIMP-RG spot analyses on 12 individual zircon grains with a range of 109.1 ± 2.8–116.7 ± 1.4 Ma. Two individual zircon ages were distinctly young (102.2 ± 3.0 Ma and 102.2 ± 2.8 Ma) compared to the rest of the sample, and thus were excluded from the error-weighted average $^{206}Pb/^{238}U$ age calculation as possibly representing new metamorphic growth (Schwartz et al., 2016). In contrast, two zircon ages were older than the rest of the sample (122.4 ± 2.4 Ma and 124.2 ± 4.6 Ma) and were also excluded from the error-weighted average $^{206}Pb/^{238}U$ age calculations as likely being xenocrysts. The error-weighted average $^{206}Pb/^{238}U$ age of the remaining zircons is 114.3 ± 2.1 (MSWD = 2.6; Fig. 6K).

***Hornblende Diorite Phase.*** SHRIMP-RG analysis of a biotite quartz diorite from Nancy Sound (sample 13NZ55A) yielded 10 individual spot analyses on 10 separate zircon grains. The individual zircon ages ranged from 111.2 ± 1.6 Ma to 120.1 ± 2.6 Ma. The error-weighted average $^{206}Pb/^{238}U$ age of all the zircons is 115.2 ± 1.9 Ma (MSWD = 1.3; Fig. 6L). Another sample from Nancy Sound, a biotite hornblende quartz diorite (sample 13NZ58), yielded eight individual SHRIMP-RG analyses on eight separate zircon grains ranging from 110.5 ± 4.4 to 116.8 ± 1.84 Ma (Fig. 6M). The error-weighted average $^{206}Pb/^{238}U$ age is 115.3 ± 1.5 Ma (MSWD = 0.5). One individual zircon age produced an age of 122.5 ± 1.8 Ma and was excluded from the error-weighted average $^{206}Pb/^{238}U$ age calculation as a probable xenocryst. A biotite hornblende diorite (sample 12NZ24) yielded eight individual SHRIMP-RG analyses on eight separate zircon grains with dates ranging from 112.4 ± 2.2 to 119.6 ± 1.8 Ma (Figs. 5 and 6N). The error-weighted average $^{206}Pb/^{238}U$ age of all the zircons is 115.8 ± 2.1 Ma (MSWD = 1.46).

Our dates are somewhat younger than an LA-MC-ICP-MS zircon date of 122.6 ± 1.9 Ma from the hornblende diorite unit along the eastern margin of the pluton reported in Allibone et al. (2009b), but overlap with another LA-MC-ICP-MS date of 114.6 ± 1.9 Ma from a hornblende diorite gneiss (Stowell et al., 2014). Older, xenocrystic(?) zircons from the latter sampled yielded a weighted average date of 119.7 ± 1.0 Ma, which also overlaps within error to the xenocrysts we observe in this and other phases of the Misty Pluton.

### *Western McKerr Intrusives*

The western McKerr Intrusives area is ~73 km$^2$, and consists of a heterogeneous suite of diorite, quartz monzodiorite, tonalite, granodiorite, and monzonite that intrude the Caswell Sound Gneiss (Bradshaw, 1985; Daczko et al., 2002; Klepeis et al., 2004; Allibone et al., 2009b). In Caswell Sound, the western McKerr Intrusives are thrust over the Misty Pluton along granulite to amphibolite facies ductile thrust faults (Daczko et al., 2002; Klepeis et al., 2004). Our sampling consists of two hornblende diorites from Caswell Sound.

A biotite hornblende diorite (13NZ34A) yielded nine individual SHRIMP-RG analyses on nine separate zircon grains with dates ranging from 108.9 ± 2.3 to 119.3 ± 1.8 Ma (Fig. 6O). One zircon date was younger than the majority (108.9 Ma), and thus was excluded from the error-weighted average $^{206}Pb/^{238}U$ age calculation. The error-weighted average $^{206}Pb/^{238}U$ age of the remaining eight zircons is 118.4 ± 0.9 Ma (MSWD = 0.4). Another hornblende diorite (13NZ35A) yielded eight individual SHRIMP-RG analyses on eight separate zircon grains with dates ranging from 113.3 ± 1.7 to 123.2 ± 2.6 Ma. The error-weighted average $^{206}Pb/^{238}U$ age of all zircons is 117.7 ± 1.6 Ma (MSWD = 2.1; Fig. 6P). These data overlap the LA-MC-ICP-MS age of 116.8 ± 3.7 Ma from a monzodiorite reported in Klepeis et al. (2004).

### *Eastern McKerr Intrusives*

The eastern McKerr Intrusives consist of ~155 km$^2$ of variably foliated, medium- to coarse-grained equigranular diorite, quartz diorite, and quartz monzodiorite (Bradshaw, 1985; Allibone et al., 2009b). Unlike other Western Fiordland Orthogneiss plutons, the eastern McKerr Intrusives contain a significant component of xenolithic granitic orthogneisses and metasedimentary rocks of unknown affinity (Bradshaw and Kimbrough, 1991). Our sampling consists of a McKerr hornblende diorite and a two-mica granitic orthogneiss from a xenolithic raft in George Sound.

A biotite hornblende diorite (15NZ20) from host diorite in George Sound yielded nine separate SHRIMP-RG spot analyses on nine individual zircon grains with dates ranging from 114.7 ± 2.6 to 124.4 ± 3.3 Ma (Fig. 6R). The error-weighted average $^{206}Pb/^{238}U$ age of all zircons is 120.1 ± 2.8 (MSWD = 1.6). Our date overlaps an existing SHRIMP zircon date of 120.0 ± 2.6 Ma reported in Hollis et al. (2004).

SHRIMP-RG analysis of a muscovite biotite granitic orthogneiss (15NZ12) from a xenolithic raft in the eastern end of George Sound yielded complex results; eight zircon spot analyses gave dates ranging from 304 ± 10 Ma to 125 ± 2.9 Ma (Fig. 6Q). Zircon dates cluster in two populations with an error-weighted average $^{206}Pb/^{238}U$ age of 128.3 ± 3.9 Ma (n = 4; MSWD = 1.6) for the younger population and an age of 288 ± 23 (n = 3; MSWD = 2.2.) for the older population. Discordant zircons from granitic orthogneisses reported in Bradshaw and Kimbrough (1991) give a similar upper intercept date of ca. 341 ± 34 Ma, although neither data set precisely constrains the age of the older population.

### *Worsley Pluton*

The Worsley Pluton is the second-most aerially extensive unit, ~569 km$^2$. It consists of a core unit of two-pyroxene diorite, monzodiorite, and monzonite that is surrounded by a hornblende diorite unit that commonly contains relict pyroxene (Bradshaw, 1985, 1989a, 1990; Allibone et al., 2009b). Our sampling consists of two samples from the two-pyroxene core (Fig. 3).

A two-pyroxene diorite (15NZ2) from Bligh Sound gave 11 zircon spot analyses from 11 grains with dates ranging from 113.7 ± 3.6 to 125.1 ± 2.7 Ma (Figs. 5 and 6S). The youngest spot is a rim and is likely metamorphic. The error-weighted average $^{206}Pb/^{238}U$ age of the remaining zircons is 121.6 ± 1.9 (MSWD = 0.7). Another two-pyroxene diorite (15NZ27) from Bligh Sound gave 13 zircon spot analyses from 12 individual grains with dates ranging from 119.3 ± 2.4 to 128.9 ± 3.5 Ma (Figs. 5 and 6T). Core and rim analyses on one grain yielded statistically indistinguishable results (124.4 ± 2.9 and 120.2 ± 2.8, respectively). The error-weighted average $^{206}Pb/^{238}U$ age of all zircons is 123.2 ± 1.6 (MSWD = 1.0). Our dates overlap with previous U-Pb zircon TIMS and SHRIMP chronology from the core unit that yielded dates of 124 ± 1.0 Ma (Tulloch and Kimbrough, 2003), 123.68 ± 0.36 Ma (A. Tulloch, 2016, personal commun.), 123.4 ± 1.1 Ma (Bolhar et al., 2008), and 121.8 ± 1.7 Ma (Hollis et al., 2004).

### Zircon Geochemistry and Thermometry

Zircons from the Western Fiordland Orthogneiss that range from ca. 124 to 114 Ma (Fig. 7) are distinguished by Th/U values >0.3, Th concentrations ranging from 4 to 1074 ppm, and U concentrations ranging from 12 to 1326 ppm (Fig. 8A). Chondrite-normalized REE patterns show pronounced positive Ce and negative Eu anomalies (Fig. 8B), and moderate to steep slopes from middle to heavy REEs (Figs. 8B, 8C). Dy/Yb is positively correlated with Th/U, consistent with intrasample fractionation trends (Fig. 8C) from a parental magma with Th/U of ~1.0 and Dy/Yb of ~0.4. Two samples from the Misty Pluton in Bradshaw Sound display distinct fractionation trends pointing toward a chemically distinct parental magma (Th/U = 3; Dy/Yb = 0.3). Corrected Ti-in-zircon temperatures for all Western Fiordland Orthogneiss zircons range from 780 to 870 °C. The mean Ti-in-zircon temperature for the Western Fiordland Orthogneiss is 838 ± 46 °C (1σ standard deviation; n = 135; Fig. 8D). Intrapluton average temperatures range from ~840 to 880 °C for the central and southern Malaspina Pluton, and ~850 °C for the northwest Malaspina Pluton; ~780–850 °C for the Misty Pluton; ~800–850 °C for the western McKerr Intrusives, ~840 °C for the eastern McKerr Intrusives, and 800–840 °C for the Worsley Pluton.

## DISCUSSION

### Identifying Igneous Zircons in Lower Arc Crust

A particular problem in quantifying tempos of lower arc construction is distinguishing zircons produced from magmatic crystallization from those produced during subsequent metamorphic or deformational events. This is particularly important for zircons in this study because the Western Fiordland Orthogneiss underwent high-temperature metamorphism (eclogite-granulite and amphibolite facies) and partial melting from 116 to 105 Ma, possibly resulting in new metamorphic growth (Oliver, 1980; Bradshaw, 1990; Klepeis et al., 2007; Allibone et al., 2009b, 2009c; Stowell et al., 2014; Schwartz et al., 2016). In this study we attempt to overcome these issues in several ways: (1) samples with clear migmatitic textures were avoided, and samples were chosen to minimize deformational and metamorphic overprints; (2) despite these attempts, some samples have granulite or amphibolite facies metamorphic assemblages (see Table 1); therefore, ion probe spots were carefully chose to avoid thin (<10 μm) luminescent rims present in some samples that are likely metamorphic in origin; (3) trace elements were collected during U-Pb analysis from all zircons to identify heavy REE depletions that may signify cocrystallization of metamorphic garnet at granulite to upper amphibolite facies conditions, and/or the presence of low Th/U domains that indicate growth in fluid-present conditions at amphibolite facies and lower temperature conditions (Harley et al., 2007; Rubatto 2002); and (4) we compare our SHRIMP-RG zircon dates to those from metamorphic zircons and titanites in paragneisses in contact aureoles of the Western Fiordland Orthogneiss (Schwartz et al., 2016), and to metamorphic garnet dates from the Western Fiordland Orthogneiss (Stowell et al., 2014), with the expectation that metamorphic dates should largely postdate igneous crystallization.

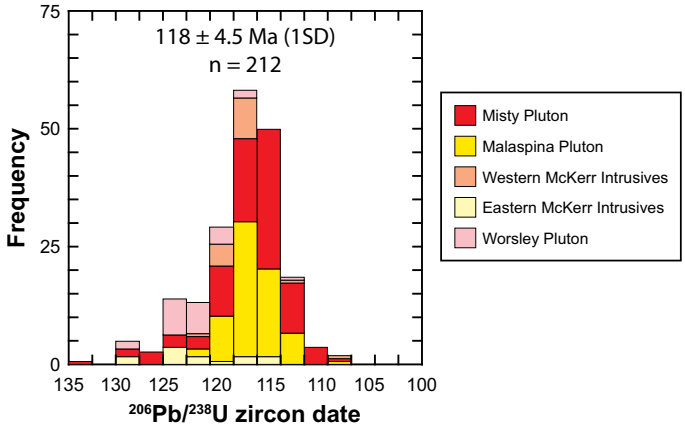


**Figure 7. Histogram of $^{206}Pb/^{238}U$ dates for the Western Fiordland Orthogneiss. Dates discussed in text as likely metamorphic or displaying open system behavior are excluded (rej.—rejected). Mean average date for all Western Fiordland Orthogneiss zircons is 118 ± 4.5 Ma (1σ standard deviation, SD; n = 212), indicating the timing of peak magmatic production in the lower crust of the Median Batholith in Fiordland.**

In general, CL imaging of zircons in this study reveals that Western Fiordland Orthogneiss zircons display weak oscillatory and sector zoning, characteristic of zircons grown from mafic to intermediate melts (Grimes et al., 2009; Schwartz et al., 2010). Trace element analyses of these domains yield chondrite-normalized REE abundances that have heavy REE enrichments and light REE depletions, pronounced positive cerium anomalies, and negative europium anomalies (Figs. 8A–8C). No Western Fiordland Orthogneiss zircons in this study display flattening of the heavy REEs that might suggest equilibrium growth in the presence of garnet (Fig. 8B).

Rubatto (2002) proposed that zircons formed during amphibolite facies metamorphism in oxidizing environments will commonly have low abundances of Th (melt insoluble) and high U concentrations (melt soluble), resulting in Th/U values <~0.1. Although several samples display amphibolite facies overprints, all zircons analyzed in this study have Th/U values >0.3 (Fig. 8A). Ti-in-zircon thermometry gives temperatures that are >750 °C, with a Western Fiordland Orthogneiss average of ~826 °C consistent with late-stage crystallization from a mafic magma. Incorporating uncertainties in the activity of $TiO_2$ also yields magmatic temperatures >~740 °C, rather than subsolidus or low-temperature metamorphic conditions temperatures predicted from pseudosection modeling (Stowell et al., 2014). Together with the lack of observed chondrite normalized heavy REE depletions, these geochemical features support the notion that Western Fiordland Orthogneiss zircons grew in equilibrium with a mafic to intermediate melt and not during granulite or amphibolite facies metamorphism.

Comparison of our SHRIMP-RG dates with those from metamorphic host rocks reveals that Western Fiordland Orthogneiss dates are generally older, but overlap with the oldest metamorphic zircon, titanites, and garnet dates from host rocks. For example, metamorphic zircons in metasedimentary rocks in the Western Fiordland Orthogneiss contact aureole yield $^{206}Pb/^{238}U$ (SHRIMP-RG) dates of 116.3–112.0 Ma (Schwartz et al., 2016) versus dates of 123.2–114.2 Ma from zircons in this study (see also dates in Gibson and Ireland, 1995; Hollis et al., 2004). Titanite laser ablation

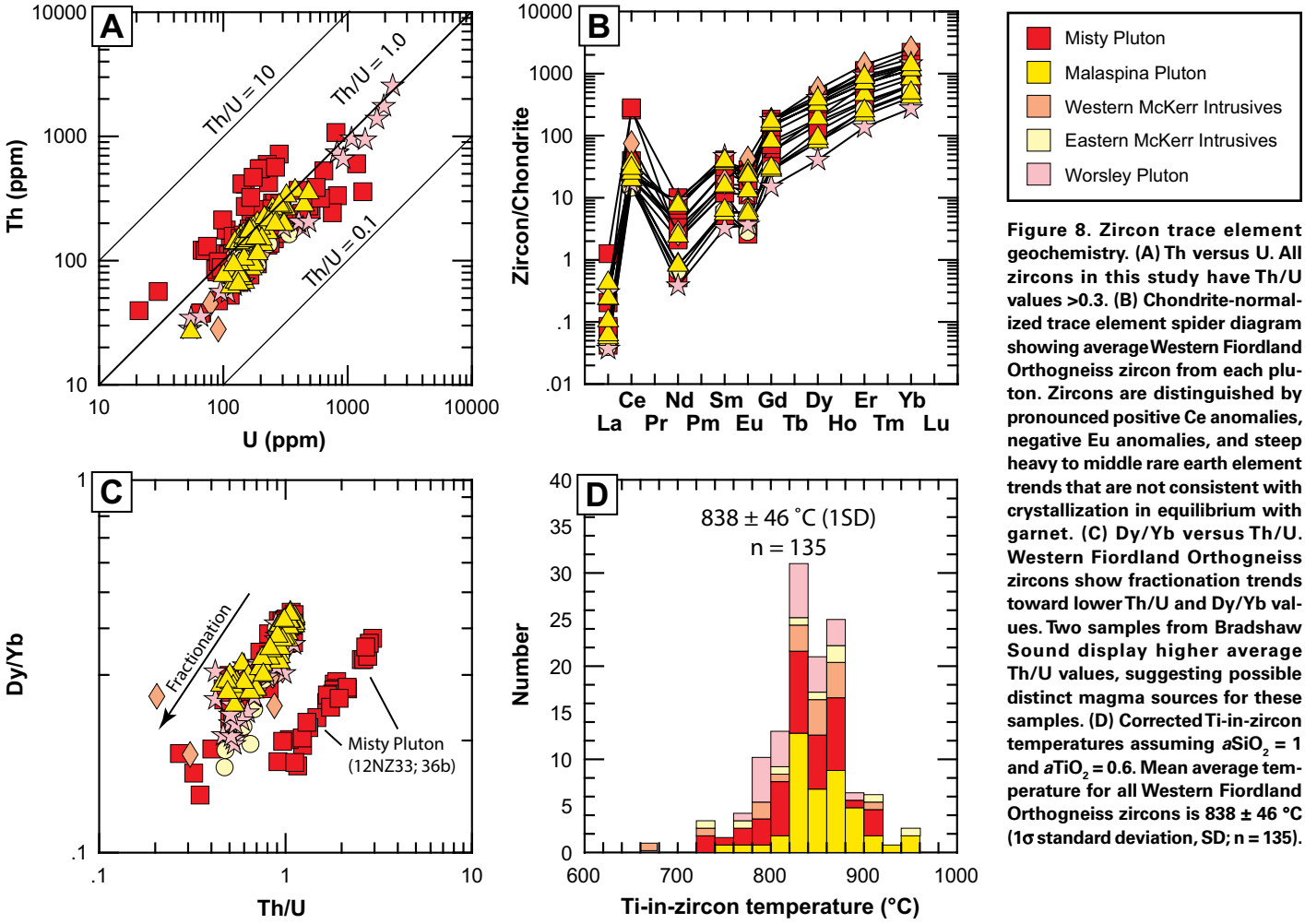


**Figure 8. Zircon trace element geochemistry. (A) Th versus U. All zircons in this study have Th/U values >0.3. (B) Chondrite-normalized trace element spider diagram showing average Western Fiordland Orthogneiss zircon from each pluton. Zircons are distinguished by pronounced positive Ce anomalies, negative Eu anomalies, and steep heavy to middle rare earth element trends that are not consistent with crystallization in equilibrium with garnet. (C) Dy/Yb versus Th/U. Western Fiordland Orthogneiss zircons show fractionation trends toward lower Th/U and Dy/Yb values. Two samples from Bradshaw Sound display higher average Th/U values, suggesting possible distinct magma sources for these samples. (D) Corrected Ti-in-zircon temperatures assuming $a\mathrm{SiO_2}$ = 1 and $a\mathrm{TiO_2}$ = 0.6. Mean average temperature for all Western Fiordland Orthogneiss zircons is 838 ± 46 °C (1σ standard deviation, SD; n = 135).**

split stream (LASS) ICP-MS chronology from the same host rocks yields dates ranging from 116.2 to 107.6 Ma (Schwartz et al., 2016). Sm-Nd garnet dates from the Western Fiordland Orthogneiss range from 115.6 ± 2.6 Ma to 110.6 ± 1.9 Ma (Stowell et al., 2014), and a minor population of metamorphic zircon rims and titanites in the Doubtful Sound region extends to even younger dates of 105.6–102.3 Ma (Schwartz et al., 2016). These metamorphic dates are in general younger than Western Fiordland Orthogneiss dates, and those that overlap likely reflect contact metamorphic heating in host rocks during batholith emplacement.

Of the 216 zircons analyzed in this study, 7 zircons were rejected as statistically younger outliers (see preceding) and these give dates ranging from 113 to 102 Ma (see Data Repository Table DR2). These dates overlap with metamorphic dates suggesting minor recrystallization or metamorphic growth. We therefore interpret the majority of zircons dates in this study as recording the timing of igneous crystallization.

### Tempos of Arc Construction

Along the southeast Gondwana margin, subduction was active for >150 m.y., resulting in the addition of large volumes of magmatic rocks that constitute the Mesozoic Median Batholith (Figs. 9, 10A, 10B, and 10C) (Mortimer et al., 1999). Like other well-studied orogenic belts, the pace of magmatic addition in the Median Batholith was not steady state, but was punctuated by high-volume magmatic pulses (Figs. 4 and 9). The largest of these pulses, or flare-ups, resulted in emplacement of the Cretaceous Separation Point Suite (including the Western Fiordland Orthogneiss plutons). Our results from the deepest level of the Median Batholith reveal that construction occurred by emplacement of several plutons starting at 128.3 ± 3.9 Ma and continuing to 114.2 ± 0.7 Ma (Fig. 9). At pluton scale, growth of the Western Fiordland Orthogneiss involved two voluminous pulses: (1) the Worsley Pluton, Breaksea Orthogneiss, and eastern McKerr Intrusives ca. 128–120 Ma, and (2) the western McKerr Intrusives, Misty and Malaspina Plutons, and Resolution Orthogneiss from ca. 120 to 114 Ma (Fig. 10D). Peak magmatic production occurred during the later interval ca. 118–115 Ma (Fig. 7), during which time ~70% of the exposed Western Fiordland Orthogneiss was emplaced into Paleozoic host rocks. Collectively, construction of the Western Fiordland Orthogneiss signifies a surge of >2300 km$^2$ of mafic to intermediate magmas into the lower crust of the Median Batholith over ~14 m.y. Apparent intrusive rates from the lower crustal portion of Fiordland peaked at ~650 km$^2$/m.y., although we note that these values do not include shallow- and mid-crustal plutons in Eastern Fiordland, Stewart Island, Westland, and other parts of the orogen in Antarctica and Australia. These data are similar in magnitude and duration to documented high-MAR events in other Cordilleran arcs that range to ~1200 km$^2$/m.y. in the Sierra Nevada and Coast Mountains Batholiths (Ducea, 2001; Ducea and Barton, 2007; DeCelles et al., 2009; Paterson et al., 2011; Ducea et al., 2015), but differ in that emplacement pressures were greater (>10 kbar; DePaoli et al., 2009; Daczko and Halpin, 2009;

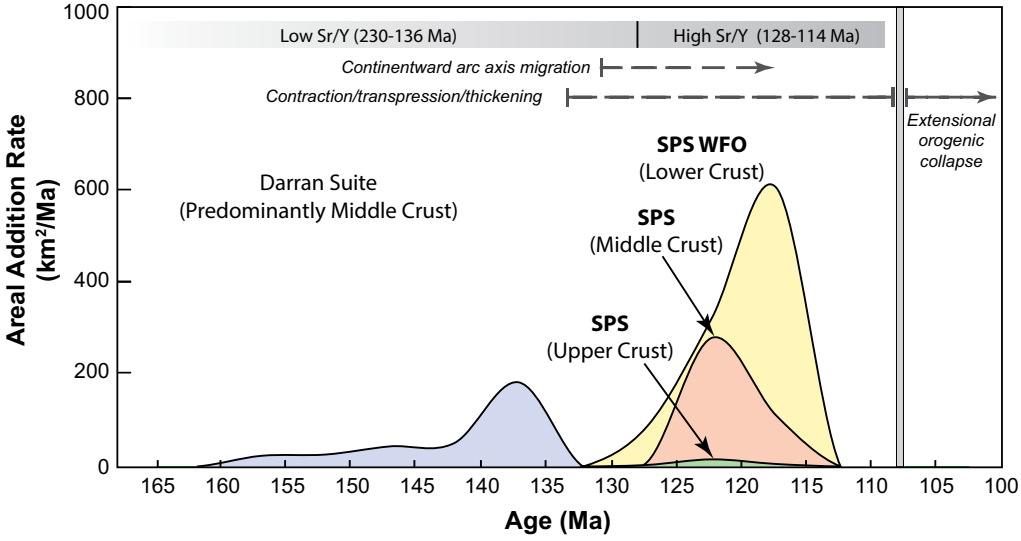


**Figure 9. Graph of apparent intrusive rates versus age for the Darran Suite and Separation Point Suite (SPS) of the Mesozoic Median Batholith. WFO—Western Fiordland Orthogneiss. Areas are calculated from surface area exposures of plutonic rocks in Turnbull et al. (2010). Submerged plutonic rocks were excluded in calculations; however, inclusion of these areas would result in slightly higher apparent intrusive rates. Ages, areas, and rates are summarized in Table 2. Separation Point Suite magmatism in the middle and upper crust includes plutons in eastern and central Fiordland, and southwestern Fiordland, respectively. Emplacement pressures for plutons were provided in Allibone et al. (2007, 2009a, 2009b), Scott et al. (2009), and references therein.**

Allibone et al., 2009b; Stowell et al., 2014) and involved predominantly mafic to intermediate diorites and monzodiorites.

The voluminous magmatic surge that characterized construction of the Western Fiordland Orthogneiss is illustrated in Figure 9, which shows areal addition rates, sometimes called apparent areal fluxes, for the Median Batholith calculated from the present-day surficial rock distributions and $^{206}Pb/^{238}U$ zircon dates (Table 2). We only consider data from the Darran and Separation Point Suites, and do not include data from A-type rocks in our analysis as their petrogenesis and significance are not well constrained (e.g., Pomona Island Granite, Fowler Granite). The high areal addition rates associated with the Western Fiordland Orthogneiss overlap temporally with mid- and shallow-crustal Separation Point Suite in eastern and southwestern Fiordland, respectively (Fig. 9). These data demonstrate that the initiation of high-Sr/Y magmatism associated with the Separation Point Suite and Western Fiordland Orthogneiss coincided with a surge of magmatism at all structural levels, particularly the lower and middle crust. It is notable that surges in high-Sr/Y magmatism occurred throughout Zealandia, in Nelson, Westland, and Stewart Island (Table 2), Queensland, Australia, and Thurston Island in East Antarctica (Kimbrough et al., 1994; Tulloch and Kimbrough, 2003). The percentage of flare-up–related Cretaceous plutonic rocks and/or host rocks also increases systematically with depth from shallow (15%) to middle (23%) to deep crustal levels (53%). Comparison of areal addition rates between the Western Fiordland Orthogneiss and other Separation Point Suite plutons in Fiordland reveals that Cretaceous plutonic activity was concentrated in the lower crust during the arc flare-up, and systematically decreased upward, consistent with observations from other Cordilleran arcs systems (e.g., Paterson et al., 2004, 2011; de Silva, 2008; Miller et al., 2009; de Silva et al., 2015). As pointed out in Tulloch and Kimbrough (2003), no volcanic rocks are associated with the Separation Point Suite, and we speculate that the absence may reflect the high $SiO_2$ contents and viscosities of the mid- to shallow-crustal Separation Point Suite rocks. High volatile contents relative to more mafic Darran Suite rocks may also have resulted in rapid degassing and crystallization, resulting in a further increase in effective viscosity.

In contrast to the single surge of magmatism recorded in the Western Fiordland Orthogneiss and wider Separation Point Suite, the older and longer lived Darran Suite displays an episodic record of magmatism with peak production occurring ca. 147–136 Ma (Kimbrough et al., 1994). Only minor volcanic rocks are preserved in the Darran Suite and they make up <5% of the exposed crust (see discussion in Kimbrough et al., 1994). Peak magmatic production is associated with emplacement of the extensive Murchison Intrusives and Darran Leucogabbro, and calculated flux values are likely minima, as other large plutonic complexes remain poorly mapped and studied (e.g., Hunter Intrusives and Lake Hankinson Complex), requiring further mapping, chemistry, and chronologic investigations to refine areal addition rates. We are thus cautious in interpretation of specific flux rates for the Darran Suite and note that these rates will likely change as more geochemical and isotopic data are collected. Despite this caveat, we note that construction of the Median Batholith in the Fiordland involved: (1) peak production of low-Sr/Y magmas in the Darran Suite from 147 to 136 Ma (Kimbrough et al., 1994); (2) abrupt termination of Darran Suite magmatism ca. 136 Ma; (3) an apparent ~8 m.y. magmatic gap from 136 to 128 Ma (Tulloch et al., 2011), and (4) a surge of high-Sr/Y magmatism in the Western Fiordland Orthogneiss and Separation Point Suite starting at 128 Ma and continuing to 114 Ma (Mattinson et al., 1986; Muir et al., 1998; Tulloch and Kimbrough, 2003; Hollis et al., 2004; Bolhar et al., 2008; Scott and Palin, 2008; this study). As noted by previous workers, this terminal surge of high-Sr/Y magmas in the Median Batholith reflects a fundamental change in magma composition with garnet playing a role as either a fractionating or residual phase (Muir et al., 1995, 1998; Tulloch and Kimbrough, 2003). Development of high-Sr/Y magmatism at all depths signifies a major transition in internal arc and/or subduction zone dynamics at this sector of the Median Batholith during the interval between 136 and 128 Ma (Tulloch and Kimbrough, 2003; Tulloch et al., 2011). We explore the tectonic significance of this transition in the following.

## Arc-Parallel and Arc-Normal Magma Focusing in the Median Batholith

To better understand possible mechanisms for the transition in arc chemistry from low- to high-Sr/Y magmatism and high magmatic production rates, we compiled published $^{206}Pb/^{238}U$ zircon dates from Fiordland to elucidate possible spatiotemporal patterns (Table 2). Results reveal that the transition from Darran Suite to Separation Point Suite magmatism was coincident with arc-normal (continentward) migration of the frontal arc axis from the Late Jurassic to the Early Cretaceous (e.g., Kimbrough et

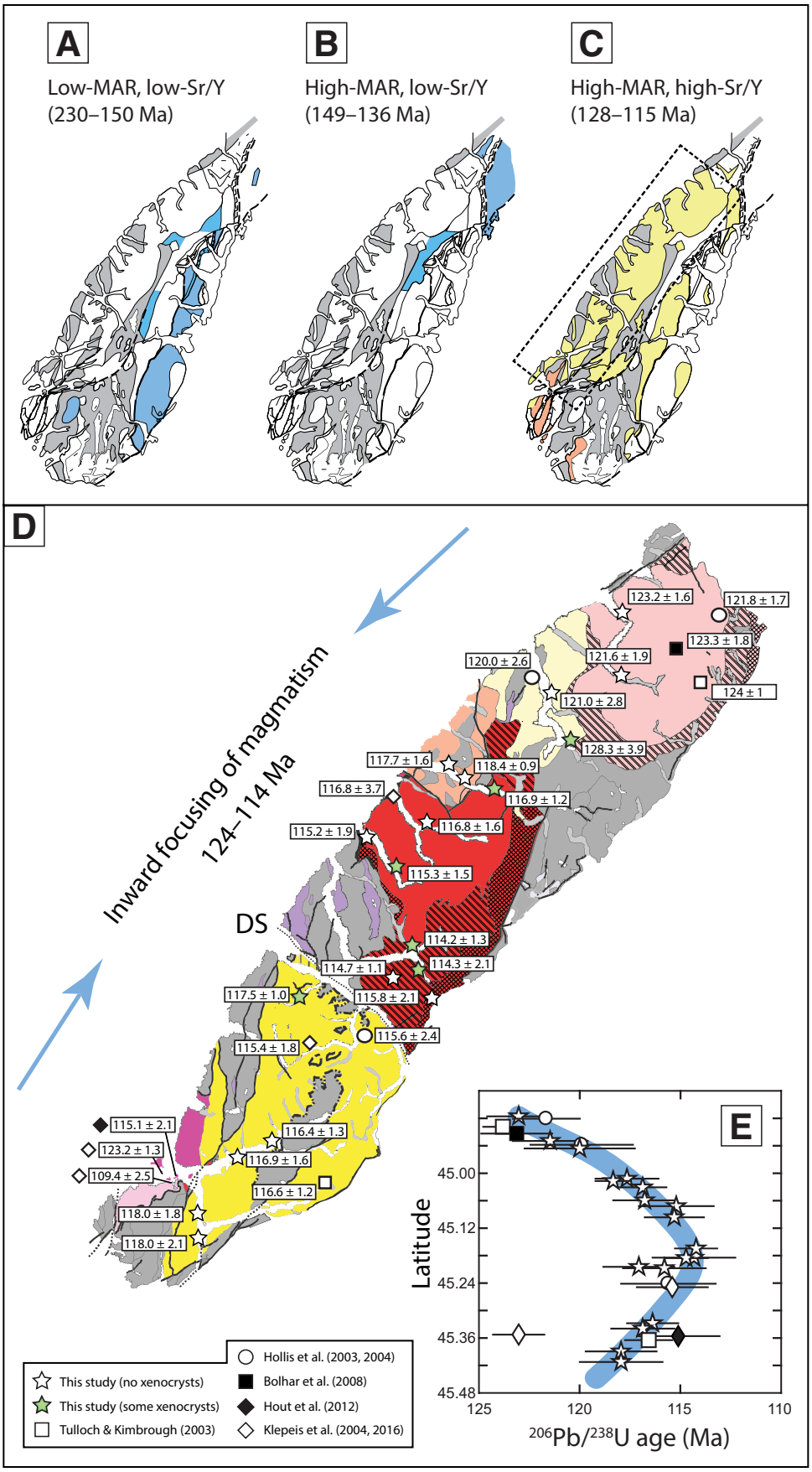


**Figure 10. Summary of the tempo of arc construction in the Fiordland sector of the Median Batholith. (A) Low-MAR (magma addition rate), low-Sr/Y magmatism persisted from ca. 230 to 150 Ma primarily in the outboard arc. (B) High-MAR, low-Sr/Y phase signifying peak magmatic flux in the outboard arc. Magmatism was coincident with possible uplift ca. 140 Ma (Spell et al., 2000), and crustal thickening in the Otago Schist (Gray and Foster, 2002). Early granulite facies metamorphism initiated ca. 134 Ma in northern Fiordland and was followed by an apparent 8 m.y. hiatus in magmatism (Tulloch et al., 2011). (C) High-MAR, high-Sr/Y magmatism renewed at all depths with the locus of peak magmatism shifted toward inboard (toward Gondwana interior). Black inset box defines area shown in D. (D) Geologic map of western Fiordland showing the spatial distribution of ion probe and thermal ionization mass spectrometry igneous zircon dates. Ages from this study are distinguished based on the presence (green stars) or absence (white stars) of xenocrystic zircons. The majority of xenocrystic zircons are located in the Misty Pluton. DS—Doubtful Sound. (E) Latitude versus date plot for the Western Fiordland Orthogneiss showing apparent trench-parallel, time-transgressive magma focusing toward the Doubtful Sound region. Thick blue line represents visually estimated best fit to data. The Breaksea Orthogneiss sample diverges from the overall age pattern.**

al., 1993; Muir et al., 1995; Tulloch and Kimbrough, 2003; Hollis et al., 2004; Klepeis et al., 2007, 2016; Bolhar et al., 2008; Scott and Palin, 2008). In eastern Fiordland, continentward migration is recorded in the temporal transition from Separation Point Suite plutonism east of the Grebe mylonite zone ca. 122 Ma (Bolhar et al., 2008) to Separation Point Suite plutonism west of the Grebe mylonite zone from 121 to 116 Ma (Scott and Palin, 2008). This migration occurred during a period of regional thrusting, transpression, and crustal thickening along the Grebe mylonite zone and Gutter shear zone (Fig. 2) (e.g., Daczko et al., 2001, 2002; Klepeis et al., 2004; Marcotte et al., 2005; Allibone and Tulloch, 2008; Scott et al., 2009, 2011). Whole-rock and zircon isotopic data suggest that neither the outboard Separation Point Suite nor inboard Western Fiordland Orthogneiss involved significant contributions of preexisting crust (McCulloch et al., 1987; Muir et al., 1995; Bolhar et al., 2008; Decker, 2016); rather, both suites were likely sourced from the mantle and/or lower plate, indicating that westward migration of the arc axis resulted from changes in subduction zone dynamics such as flattening of the underlying slab.

Compiled zircon dates within the Western Fiordland Orthogneiss reveal a pattern of time-transgressive, inward magmatic younging toward Doubtful Sound (Fig. 10D). Consideration of Figure 10D shows that the oldest dates in the Western Fiordland Orthogneiss are located in the northern Worsley Pluton (124–121 Ma; Hollis et al., 2004; Tulloch and Kimbrough, 2003; Bolhar et al., 2008), the eastern McKerr Intrusives (ca. 128 Ma), the southern Breaksea Orthogneiss (ca. 123 Ma; Hout et al., 2012; Klepeis et al., 2016), and the easternmost Misty Pluton (123 Ma; Allibone et al., 2009b). Plutonic rocks between these regions, particularly in the Misty and Malaspina Plutons, become progressively younger toward the Doubtful Sound region; the youngest dates in this study (ca. 114 Ma) are from Bradshaw Sound (Figs. 10D, 10E). Interpretation of these data in terms of Cretaceous arc tempos is complicated by several factors, including uncertainties in igneous emplacement depth and postemplacement modification by multiple phases of deformation related to Cretaceous extensional orogenic collapse and Cenozoic normal faulting. In general, emplacement pressures are poorly constrained due to the effects of post–igneous emplacement granulite and amphibolite facies recrystallization. Historically, the presence of relict igneous orthopyroxene in the Western Fiordland Orthogneiss has been interpreted to signify mid-crust igneous emplacement depths (Bradshaw, 1989c; Clarke et al., 2000); however, more recent studies have argued that orthopyroxene stability may be more a function of redux conditions of the magma rather than pressure conditions (Chapman et al., 2015). Studies of igneous emplacement depths based on thermobarometry of contact metamorphic assemblages indicate intrusion at depths equivalent to 10 and 14 kbar (Malaspina Pluton; Allibone et al., 2009c); however, these contact assemblages are rare and their occurrence and distribution are insufficient to identify systematic correlations between depth of emplacement and crystallization age.

Tectonic modification of the crustal structure of western Fiordland is also an important consideration in evaluating temporal magmatic patterns. By ca. 106 Ma, ductile normal faulting associated with the development of the Doubtful Sound shear zone (Gibson et al., 1988; Oliver, 1980) moved the Misty Pluton (hanging wall) down and to the northeast relative to the Malaspina Pluton (footwall) in a direction oblique to the overall trend of the arc (Klepeis et al., 2007, 2016). Garnet thermobarometry data from the Misty and Malaspina Plutons indicate <6.5 km of rock thickness excised along the Doubtful Sound shear zone (Stowell et al., 2013, 2014). Consequently, restoration of crust prior to the formation of this shear zone places the southern part of the Misty Pluton structurally above the northern part of the Malaspina Pluton, with a net effect of shrinking the zone of focused magmatic younging around the Doubtful Sound region. Cenozoic normal faulting localized along fiords also resulted in vertical movement of plutonic blocks (Turnbull et al., 1993; Sutherland and Melhuish, 2000; King et al., 2008). Excision of rock is estimated to be <6.5 km of rock thickness; therefore, Cenozoic vertical fault motion is not expected to disrupt the overall age pattern.

With these considerations in mind, we interpret the distribution of igneous zircon dates as preserving a pattern of arc-parallel magma focusing that was progressively concentrated toward the interior of the Western Fiordland Orthogneiss pluton belt, resulting in the emplacement of the three large, compositional and temporally zoned, plutons (Misty, Malaspina, and Worsley Plutons). At pluton scale, magma focusing in the Malaspina Pluton led to incremental pluton growth by repeated injections of sheets of dioritic magmas that were fed from a 6-km-wide zone of focused diking in its northwest sector (Klepeis et al., 2016). Similar patterns of inward magma focusing are observed in nested plutonic complexes in other Cordilleran orogenic belts (e.g., Tuolumne Batholith, North Cascades plutonic complex). For example, in the Tuolumne Batholith, magma focusing involved repeated input of heat over time, leading to the creation of a focused magma plumbing system that was enhanced by convection, mixing, and fractional crystallization (e.g., Bateman and Chappell, 1979; Coleman et al., 2004; Matzel et al., 2006; Memeti et al., 2010; Paterson et al., 2011). The dimensions of the Tuolumne Batholith are nearly identical to each of three large individual plutons in the Western Fiordland Orthogneiss (Worsley, Misty, and Malaspina); thus the magnitude of magmatic focusing we observe is ~3× greater in length versus the Tuolumne Batholith when measured parallel to the paleoarc axis. Focusing over a broader area in the lower crust was likely enhanced by unusually high heat flow from the underlying mantle associated with a surge of mafic to intermediate magmas. Diking and vertical diapiric movements in channels and horizontal sheeting were instrumental in transferred heat and mantle-derived melts during sustained high-flux magmatism from 128 to 114 Ma (Klepeis et al., 2016).

### Zircon Inheritance and the Plutonic Architecture of Western Fiordland

Patterns of zircon inheritance also reveal information about the crustal structure beneath the Western Fiordland Orthogneiss and processes of batholith construction during the Separation Point Suite high-MAR event. Our zircon data show little evidence for pre-Cretaceous Mesozoic basement beneath the Western Fiordland Orthogneiss. In general, zircon populations are remarkably homogeneous with few examples of overdispersion in dates (i.e., MSWD values are typically <2.0). Four samples from the Misty Pluton and one sample from the Malaspina Pluton contain minor xenocrystic zircons that give Western Fiordland Orthogneiss ages of 128 Ma or younger, indicating recycling of older Western Fiordland Orthogneiss plutonic rocks during batholith construction (see green stars in Fig. 10D). Sample 13NZ36b is the most complex of these Misty Pluton samples and contains possibly two xenocrystic populations with deconvolved dates of ca. 119.7 and 127.9 Ma. The former dates are identical to those for xenocrystic zircons reported from the Misty Pluton sample in Stowell et al. (2014). The ca. 128 Ma date may indicate recycling of early Western Fiordland Orthogneiss plutons (e.g., Mount Edgar Pluton, Supper Cove, and Omaki Orthogneisses, and portions of the eastern McKerr Intrusives; see Table 2 and references therein). We note that no Jurassic–Triassic zircons were observed in our data set, despite models that invoke underthrusting and melting of Darran Suite plutonic rocks to generate the Western Fiordland Orthogneiss (e.g., Muir et al., 1998).

Zircons from the raft of granitic orthogneiss enveloped within the eastern McKerr Intrusives (15NZ12) give a date of 128 Ma for the youngest zircon population, similar to the age of other early Western Fiordland Orthogneiss plutons and xenocrystic zircons in the Misty Pluton. As

noted by Bradshaw and Kimbrough (1991), we also observe discordant Paleozoic zircons, in this case Permian or older xenocrysts, that do not occur in other Western Fiordland Orthogneiss samples. Decker (2016) reported that both Cretaceous and older zircons in this sample are characterized by negative $\delta^{18}O$ (zircon) values unlike any other zircon analyzed from the Western Fiordland Orthogneiss (5.76 ± 0.04‰; n = 126). Light $\delta^{18}O$ (whole rock) values have been reported in Permian–Triassic rocks located ~25–30 km to the east of the head of George Sound (Blattner and Williams, 1991). One interpretation is that portions of these rocks may have been underthrusted beneath western Fiordland and incorporated into early Western Fiordland Orthogneiss magmas. The extent of these rocks beneath the Western Fiordland Orthogneiss is unknown, but they are likely minor, as Western Fiordland Orthogneiss plutonic rocks are distinct in $\delta^{18}O$ (zircon) values. We also note that large rafts of granitic orthogneiss that typify portions of the eastern McKerr Intrusives are not reported from other Western Fiordland Orthogneiss plutons (cf. Allibone et al., 2009b). An alternative interpretation is that older xenocrystic zircons represent assimilation of the nearby ca. 318 Ma plutons (Ramenzani and Tulloch, 2009); however, it is unknown whether zircons from these rocks also have negative $\delta^{18}O$ (zircon) values.

### Episodicity and Feedbacks between Magmatism and Deformation in the Zealandia Cordillera

Our new zircon dates together with existing information indicate that construction of the Median Batholith involved a prolonged (~150 m.y.) period of episodic magmatism from 260 to 114 Ma that resulted in at least two surges of magmatism ca. 147–136 Ma and 128–114 Ma. (Figs. 10A–10C). Both surges lasted 10–14 m.y., but differ in that they involved chemically distinct magmas consisting of low-Sr/Y and high-Sr/Y plutons, respectively. The latter surge of magmatism resulted in emplacement of the Separation Point Suite, including the Western Fiordland Orthogneiss, shortly before termination of arc magmatism and the initiation of extensional orogenic collapse in this sector of the Median Batholith ca. 108–106 Ma. Like Cordilleran orogenic systems in North and South America (Ducea, 2001; Ducea and Barton, 2007; DeCelles et al., 2009), we also observe possible cyclical variations in magmatic fluxes, but in Zealandia high-MAR events are restricted to only 2 recognized pulses of chemically distinct magmas that are separated by an apparent 8 m.y. hiatus in magmatism (Tulloch et al., 2011). Although the timing between each high-MAR event gives an apparent ~20 m.y. periodicity similar to cycles in the Andean orogen (Pepper et al., 2016), it is not clear that the causal mechanisms are related and it is more likely that they are independent. For example, the terminal pulse of magmatism in the Darran Suite from 147 to 136 Ma is not strongly linked to known deformational events, although previous studies have noted possible uplift ca. 140 Ma (Spell et al., 2000), and crustal thickening from ca. 150 to 120 Ma (Gray and Foster, 2004; Little et al., 1999). Tulloch et al. (2011) also observed widespread recrystallization of metamorphic zircon ca. 134 Ma associated with the initiation of granulite facies conditions in northern Fiordland. They speculate that high-temperature metamorphism, partial melting, and emplacement of A-type plutons at that time may have been triggered by a thermal event related to either a slab breakoff or rollback event.

In contrast, stronger links exist between magmatism and deformation during the surge of Separation Point Suite magmatism. This pulse was associated temporally with (1) transpression and regional thrusting from ca. 130 to 105 Ma (Daczko et al., 2001, 2002; Marcotte et al., 2005; Klepeis et al., 2004; Allibone and Tulloch, 2008), (2) crustal thickening and possibly loading of the Western Fiordland Orthogneiss from 128 to 116 Ma (Brown, 1996; Scott et al., 2009, 2011), (3) initiation of voluminous, high-Sr/Y magmatism ca. 128 Ma (Muir et al., 1998; Tulloch and Kimbrough, 2003; Bolhar et al., 2008; this study), and (4) continentward migration of arc magmatism in the Fiordland sector of Zealandia related to flattening of the slab or changes in subduction zone geometry. These data point to a major transition in subduction zone dynamics at this sector of the Median Batholith during the interval from 136 to 128 Ma; however, the cause of this transition remains uncertain.

Scott et al. (2011) postulated that contractional thickening from 128 to 116 Ma resulted from closure of an outboard fringing arc during a period of slab advancement, although they noted that no ophiolitic fragments or mélange terranes have been observed at the putative arc-continent suture zone (Grebe mylonite zone). Alternatively, Tulloch and Kimbrough (2003) proposed that intra-arc contraction resulted from shallowing of the subducting slab producing (1) underthrusting of the outboard (Darran Suite) arc beneath the Western Fiordland Orthogneiss, (2) cessation of low-Sr/Y magmatism by continentward migration of the frontal arc axis, and (3) a single, voluminous burst of high-Sr/Y magmatism. Zircon data presented here are consistent with the Tulloch and Kimbrough (2003) model and the temporal migration of the frontal arc axis during the terminal high-MAR event. Similar patterns of magmatism and arc migration are observed in the northern Chilean segment of the Andean orogenic belt where pre-Neogene and Neogene magmatic rocks show patterns of increasing La/Yb and Sr and Nd isotopic enrichment, eastward-migration of magmatism toward the continental interior, and apparent gaps in arc magmatism lasting 5–10 m.y. (Haschke et al., 2002, 2006). These patterns are interpreted to reflect repeated cycles of slab shallowing, followed by slab breakoff or rollback with increasing incorporation of crustal material toward the end of each cycle (Haschke et al., 2002, 2006; Pepper et al., 2016). These observations support recognized trends in some segments of Andean orogenic belts toward more evolved isotopic values as a consequence of increased shortening and crustal thickening resulting in enhanced crustal melting (Haschke et al., 2002, 2006; Kay et al., 2005; DeCelles et al., 2009; Ramos, 2009; Ramos et al., 2014; DeCelles and Graham, 2015).

A key difference between the Zealandia flare-up documented here and the internally forced models for the evolution of the Mesozoic North American and South American Cordilleras is the limited role of upper plate material in triggering the terminal flare-up event. Although data are limited, existing whole-rock and zircon oxygen isotopic data indicate that the surge of mafic to intermediate magmas in the Western Fiordland Orthogneiss originated from the mantle with little to no input from evolved crustal sources (Decker, 2016). More complete geochemical data are required to better understand the triggering mechanisms for the Zealandia high-MAR event; however, existing data indicate strongly point to dynamic mantle processes such as a ridge subduction or slab-breakoff event. An implication of this observation is that high-MAR events in arcs may ultimately be sourced from the underlying mantle, and that minor crustal recycling observed in some late-stage, deep crustal magmas in the Western Fiordland Orthogneiss (Milan et al., 2016) and strongly crustal signatures in shallower level plutons in Cordilleran orogenic belts reflect intracrustal partial melting due to elevated geothermal gradients resulting from increasing mantle melt influx to the base of the crust, and/or assimilation of mantle-derived and hybrid magmas during ascent through the crustal column.

## CONCLUSIONS

Zircon chronology from the Fiordland sector of the Median Batholith document a surge of mafic to intermediate magmas that were emplaced into the lower crust during a 10 m.y. period from 124 to 114 Ma. This high-MAR event marks the termination of a prolonged period (~150 m.y.) of magmatism in the Median Batholith that lasted from ca. 260 to 114 Ma.

A major transition in magma chemistry and arc tempo occurred at 128 Ma, and was associated with a surge of high-Sr/Y magmatism at all crustal depths. Regional compilations of zircon dates show that the brief surge of magmatism immediately preceded extensional orogenic collapse at 108–106 Ma and was linked to (1) transpression and regional thrusting from ca. 130 to 105 Ma, (2) crustal thickening and possibly loading of the Western Fiordland Orthogneiss from 128 to 116 Ma, (3) initiation of voluminous, high-Sr/Y magmatism ca. 128 Ma, and (4) continentward migration of arc magmatism in the Fiordland sector of Zealandia. These features point to a major transition in subduction zone dynamics at this sector of the Median Batholith likely resulting from flattening of the slab and/or changes in subduction zone geometry. Like Cordilleran orogenic systems in North America and South America (Ducea, 2001; Ducea and Barton, 2007; DeCelles et al., 2009), we also observe cyclical variations in magmatic fluxes with an ~20 m.y. periodicity between high-MAR events; however, links and causal relationships between magmatism and deformation are not clear in the Median Batholith and surges were likely independent. Our observations coupled with limited isotopic data strongly support an externally triggered, mantle-generated process leading to the surge of magmatism from 128 to 114 Ma with only limited contributions from evolved lithospheric sources.

**ACKNOWLEDGMENTS**

We acknowledge stimulating discussions with Nick Mortimer, Dave Kimbrough, and Robinson Cecil. Schwartz thanks Carol Zamora, Hannah Shamloo, Meghann Decker, Samantha Gebauer, and John Wiesenfeld for assistance in zircon dating. We thank Dick Heermance for assistance with ArcGIS (https://www.arcgis.com/). Reviews by James Scott, George Gehrels, and an anonymous reviewer significantly improved our manuscript. We also thank Brad Ito (Stanford–U.S. Geological Survey SHRIMP-RG Lab) for keeping the sensitive high-resolution ion microprobe working so well and efficiently. We thank Richard and Mandy Abernethy and the Crew of Fiordland Expeditions for assistance with rock sampling on the Fiordland coast. The New Zealand Department of Conservation, Te Anau office is also thanked for allowing access and sampling in Fiordland. Financial support for this work was provided by National Science Foundation grants EAR-1352021 (Schwartz), EAR-1119039 (Stowell and Schwartz), and EAR-1119248 (Klepeis).

**REFERENCES CITED**

Allibone, A.H., and Tulloch, A.J., 2004, Geology of the plutonic basement rocks of Stewart Island, New Zealand: New Zealand Journal of Geology and Geophysics, v. 47, p. 233–256, doi:10.1080/00288306.2004.9515051.

Allibone, A.H., and Tulloch, A.J., 2008, Early Cretaceous dextral transpressional deformation within the Median Batholith, Stewart Island, New Zealand: New Zealand Journal of Geology and Geophysics, v. 51, p. 115–134, doi:10.1080/00288300809509854.

Allibone, A.H., Turnbull, I.M., Tulloch, A.J., and Cooper, A.F., 2007, Plutonic rocks of the Median Batholith in southwest Fiordland, New Zealand: Field relations, geochemistry, and correlation: New Zealand Journal of Geology and Geophysics, v. 50, p. 283–314, doi:10.1080/00288300709509838.

Allibone, A.H., Jongens, R., Scott, J.M., Tulloch, A.J., Turnbull, I.M., Cooper, A.F., Powell, N.G., Ladley, E.B., King, R.P., and Rattenbury, M.S., 2009a, Plutonic rocks of the Median Batholith in eastern and central Fiordland, New Zealand: Field relations, geochemistry, correlation, and nomenclature: New Zealand Journal of Geology and Geophysics, v. 52, p. 101–148, doi:10.1080/00288300909509882.

Allibone, A.H., Jongens, R., Turnbull, I.M., Milan, L.A., Daczko, N.R., DePaoli, M.C., and Tulloch, A.J., 2009b, Plutonic rocks of Western Fiordland, New Zealand: Field relations, geochemistry, correlation, and nomenclature: New Zealand Journal of Geology and Geophysics, v. 52, p. 379–415, doi:10.1080/00288306.2009.9518465.

Allibone, A.H., Milan, L.A., Daczko, N.R., and Turnbull, I.M., 2009c, Granulite facies thermal aureoles and metastable amphibolite facies assemblages adjacent to the Western Fiordland Orthogneiss in southwest Fiordland, New Zealand: Journal of Metamorphic Geology, v. 27, p. 349–369, doi:10.1111/j.1525-1314.2009.00822.x.

Armstrong, R.L., 1988, Mesozoic and early Cenozoic magmatic evolution of the Canadian Cordillera, *in* Clark, S.P., Jr., et al., eds., Processes in continental lithospheric deformation Geological Society of America Special Paper 218, p. 55–92, doi:10.1130/SPE218-p55.

Bateman, P.C., and Chappell, B.W., 1979, Crystallization, fractionation, and solidification of the Tuolumne Intrusive Series, Yosemite National Park, California: Geological Society of America Bulletin, v. 90, p. 465–482, doi:10.1130/0016-7606(1979)90<465:CFASOT>2.0.CO;2.

Blattner, P., and Williams, J.G., 1991, The Largs high-latitude oxygen isotope anomaly (New Zealand) and climatic controls of oxygen isotopes in magma: Earth and Planetary Science Letters, v. 103, p. 270–284, doi:10.1016/0012-821X(91)90166-F.

Bolhar, R., Weaver, S.D., Palin, J.M., Cole, J.W., and Paterson, L.A., 2008, Systematics of zircon crystallisation in the Cretaceous Separation Point Suite, New Zealand, using U/Pb isotopes, REE and Ti geothermometry: Contributions to Mineralogy and Petrology, v. 156, p. 133–160, doi:10.1007/s00410-007-0278-5.

Bradley, D.C., 2011, Secular trends in the geologic record and the supercontinent cycle: Earth-Science Reviews, v. 108, p. 16–33, doi:10.1016/j.earscirev.2011.05.003.

Bradshaw, J.Y., 1985, Geology of the northern Franklin Mountains, northern Fiordland, New Zealand, with emphasis on the origin and evolution of Fiordland granulites [Ph.D. thesis]: Dunedin, New Zealand, University of Otago, 379 p.

Bradshaw, J.D., 1989a, Cretaceous geotectonic patterns in the New Zealand region: Tectonics, v. 8, p. 803–820, doi:10.1029/TC008i004p00803.

Bradshaw, J.Y., 1989b, Early Cretaceous vein-related garnet granulite in Fiordland, southwest New Zealand: A case for infiltration of mantle-derived $CO_2$-rich fluids: Journal of Geology, v. 97, p. 697–717, doi:10.1086/629353.

Bradshaw, J.Y., 1989c, Origin and metamorphic history of an Early Cretaceous polybaric granulite terrain, Fiordland, southwest New Zealand: Contributions to Mineralogy and Petrology, v. 103, p. 346–360, doi:10.1007/BF00402921.

Bradshaw, J.Y., 1990, Geology of crystalline rocks of northern Fiordland: Details of the granulite facies Western Fiordland Orthogneiss and associated rock units: New Zealand Journal of Geology and Geophysics, v. 33, p. 465–484, doi:10.1080/00288306.1990.10425702.

Bradshaw, J.Y., and Kimbrough, D.L., 1991, Mid Paleozoic age of granitoids in enclaves within Early Cretaceous granulites, Fiordland, southwest New Zealand: New Zealand Journal of Geology and Geophysics, v. 34, p. 455–469, doi:10.1080/00288306.1991.9514483.

Brown, E., 1996, High-pressure metamorphism caused by magma loading in Fiordland, New Zealand: Journal of Metamorphic Geology, v. 14, p. 441–452, doi:10.1046/j.1525-1314.1996.06024.x.

Cao, W., Paterson, S., Memeti, V., Mundil, R., Anderson, J.L., and Schmidt, K., 2015, Tracking paleodeformation fields in the Mesozoic central Sierra Nevada arc: Implications for intra-arc cyclic deformation and arc tempos: Lithosphere, v. 7, p. 296–320, doi:10.1130/L389.1.

Chapman, A.D., Saleeby, J.B., and Eiler, J., 2013, Slab flattening trigger for isotopic disturbance and magmatic flare-up in the southernmost Sierra Nevada batholith, California: Geology, v. 41, p. 1007–1010, doi:10.1130/G34445.1.

Chapman, T., Clarke, G.L., Daczko, N.R., Piazolo, S., and Rajkumar, A., 2015, Orthopyroxene–omphacite- and garnet–omphacite-bearing magmatic assemblages, Breaksea Orthogneiss, New Zealand: Oxidation state controlled by high-P oxide fractionation: Lithos, v. 216–217, p. 1–16, doi: 10.1016/j.lithos.2014.11.019.

Clarke, G.L., Klepeis, K.A., and Daczko, N.R., 2000, Cretaceous high-P granulites at Milford Sound, New Zealand: Metamorphic history and emplacement in a convergent margin setting: Journal of Metamorphic Geology, v. 18, p. 359–374, doi:10.1046/j.1525-1314.2000.00259.x.

Coleman, D.S., Gray, W., and Glazner, A.F., 2004, Rethinking the emplacement and evolution of zoned plutons: Geochronologic evidence for incremental assembly of the Tuolumne Intrusive Suite, California: Geology, v. 32, p. 433–436, doi:10.1130/G20220.1.

Condie, K.C., and Kroner, A., 2013, The building blocks of continental crust: Evidence for a major change in the tectonic setting of continental growth at the end of the Archean: Gondwana Research, v. 23, p. 394–402, doi:10.1016/j.gr.2011.09.011.

Corfu, F., Hanchar, J.M., Hoskin, P.W.O., and Kinny, P., 2003, Atlas of zircon textures: Reviews in Mineralogy and Geochemistry, v. 53, p. 469–500, doi:10.2113/0530469.

Cui, Y., and Russell, J.K., 1995, Nd-Sr-Pb isotopic studies of the southern Coast Plutonic Complex, southwestern British Columbia: Geological Society of America Bulletin, v. 107, p. 127–138, doi:10.1130/0016-7606(1995)107<0127:NSPISO>2.3.CO;2.

Daczko, N.R., and Halpin, J.A., 2009, Evidence for melt migration enhancing recrystallization of metastable assemblages in mafic lower crust, Fiordland, New Zealand: Journal of Metamorphic Geology, v. 27, p. 167–185, doi:10.1111/j.1525-1314.2009.00811.x.

Daczko, N.R., Klepeis, K.A., and Clarke, G.L., 2001, Evidence of early Cretaceous collisional-style orogenesis in Northern Fiordland, New Zealand and its effects on the evolution of the lower crust: Journal of Structural Geology, v. 23, p. 693–713, doi:10.1016/S0191-8141(00)00130-9.

Daczko, N.R., Clarke, G.L., and Klepeis, K.A., 2002, Kyanite-paragonite-bearing assemblages, northern Fiordland, New Zealand: Rapid cooling of the lower crustal root to a Cretaceous magmatic arc: Journal of Metamorphic Geology, v. 20, p. 887–902, doi:10.1046/j.1525-1314.2002.00421.x.

DeCelles, P.G., and Graham, S.A., 2015, Cyclical processes in the North American Cordilleran orogenic system: Geology, v. 43, p. 499–502, doi:10.1130/G36482.1.

DeCelles, P.G., Ducea, M.N., Kapp, P., and Zandt, G., 2009, Cyclicity in Cordilleran orogenic systems: Nature Geoscience, v. 2, p. 251–257, doi:10.1038/ngeo469.

Decker, M., 2016, Triggering mechanisms for a magmatic flare-up of the lower crust in Fiordland, New Zealand, from U-Pb zircon geochronology and O-Hf zircon geochemistry [M.S. thesis]: Northridge, California State University, 122 p.

De Paoli, M.C., Clarke, G.L., Klepeis, K.A., Allibone, H., and Turnbull, I.M., 2009, The eclogite-granulite transition: Mafic and intermediate assemblages at Breaksea sound, New Zealand: Journal of Petrology, v. 50, p. 2307–2343, doi:10.1093/petrology/egp078.

de Silva, S., 2008, Arc magmatism, calderas, and supervolcanoes: Geology, v. 36, p. 671–672, doi:10.1130/focus082008.1.

de Silva, S.L., Riggs, N.R., and Barth, A.P., 2015, Quickening the pulse: Fractal tempos in continental arc magmatism: Elements, v. 11, p. 113–118, doi:10.2113/gselements.11.2.113.

Ducea, M.N., 2001, The California arc: GSA Today, v. 11, p. 4–10, doi:10.1130/1052-5173(2001)011<0004:TCATGB>2.0.CO;2.

Ducea, M.N., 2002, Constraints on the bulk composition and root foundering rates of continental arcs: A California arc perspective: Journal of Geophysical Research, v. 107, p. ECV 15-1–ECV 15-13, doi:10.1029/2001JB000643.

Ducea, M.N., and Barton, M.D., 2007, Igniting flare-up events in Cordilleran arcs: Geology, v. 35, p. 1047–1050, doi:10.1130/G23898A.1.

Ducea, M.N., Paterson, S.R., and DeCelles, P.G., 2015, High-volume magmatic events in subduction systems: Elements, v. 11, p. 99–104, doi:10.2113/gselements.11.2.99.

Eberhart-Phillips, D., and Reyners, M., 2001, A complex, young subduction zone imaged by three-dimensional seismic velocity, Fiordland, New Zealand: Geophysical Journal International, v. 146, p. 731–746, doi:10.1046/j.0956-540x.2001.01485.x.

Ferry, J.M., and Watson, E.B., 2007, New thermodynamic models and revised calibrations for the Ti-in-zircon and Zr-in-rutile thermometers: Contributions to Mineralogy and Petrology, v. 154, p. 429–437, doi:10.1007/s00410-007-0201-0.

Gehrels, G.E., et al., 2009, U-Th-Pb geochronology of the Coast Mountains batholith in north-coastal British Columbia: Constraints on age and tectonic evolution: Geological Society of America Bulletin, v. 121, p. 1341–1361, doi:10.1130/B26404.1.

Gibson, G.M., and Ireland, T.R., 1995, Granulite formation during continental extension in Fiordland, New Zealand: Nature, v. 375, p. 479–482, doi:10.1038/375479a0.

Gibson, G.M., McDougall, I., and Ireland, T.R., 1988, Age constraints on metamorphism and the development of a metamorphic core complex in Fiordland, southern New Zealand: Geology, v. 16, p. 405–408, doi: 10.1130/0091-7613(1988)016<0405:ACOMAT>2.3.CO;2.

Gollan, M., Palin, J.M., Faure, K., and Harris, C., 2005, Early Cretaceous upper crustal magmatism in southwest Fiordland: Geochronological and geochemical highlights, *in* Pettinga, J.R., and Wandres, A. eds., Geological Society of New Zealand 50th Annual Conference: Programme and Abstracts: Takaka, Geological Society of New Zealand Miscellaneous Publication 119A, p. 30.

Gray, D.R., and Foster, D.A., 2004, $^{40}Ar/^{39}Ar$ thermochronologic constraints on deformation, metamorphism and cooling/exhumation of a Mesozoic accretionary wedge, Otago Schist, New Zealand: Tectonophysics, v. 385, p. 181–210, doi:10.1016/j.tecto.2004.05.001.

Grimes, C.B., John, B.E., Cheadle, M.J., Mazdab, F.K., Wooden, J.L., Swapp, S., and Schwartz, J.J., 2009, On the occurrence, trace element geochemistry, and crystallization history of zircon from in situ ocean lithosphere: Contributions to Mineralogy and Petrology, v. 158, p. 757–783, doi:10.1007/s00410-009-0409-2.

Grove, M., Bebout, G.E., Jacobson, C.E., Barth, A.P., Kimbrough, D.L., King, R.L., Zou, H., Lovera, O.M., Mahoney, B.J., and Gehrels, G.E., 2008, The Catalina Schist: Evidence for middle Cretaceous subduction erosion of southwestern North America, *in* Draut, A.E., et al., eds., Formation and applications of the sedimentary record in arc collision zones: Geological Society of America Special Paper 436, p. 335–361, doi:10.1130/2008.2436(15).

Harley, S.L., Kelly, N.M., and Möller, A., 2007, Zircon behaviour and the thermal histories of mountain chains: Elements, v. 3, p. 25–30, doi:10.2113/gselements.3.1.25.

Haschke, M.R., Scheuber, E., Gunther, A., and Reutter, K.-J., 2002, Evolutionary cycles during the Andean orogeny: Repeated slab breakoff and flat subduction?: Terra Nova, v. 14, p. 49–55, doi:10.1046/j.1365-3121.2002.00387.x.

Haschke, M., Gunther, A., Melnick, D., Echtler, H., Reutter, K.J., Scheuber, E., and Oncken, O., 2006, Central and southern Andean tectonic evolution inferred from arc magmatism, *in* Oncken, O., et al., eds., The Andes—Active subduction orogeny: Frontiers in Earth Sciences 1: Berlin, Springer-Verlag, p. 337–353, doi:10.1007/978-3-540-48684-8_16.

Hildreth, W., and Moorbath, S., 1988, Crustal contributions to arc magmatism in the Andes of Central Chile: Contributions to Mineralogy and Petrology, v. 98, p. 455–489, doi:10.1007/BF00372365.

Hollis, J.A., Clarke, G.L., Klepeis, K.A., Daczko, N.R., and Ireland, T.R., 2003, Geochronology and geochemistry of high-pressure granulites of the Arthur River Complex, Fiordland, New Zealand: Cretaceous magmatism and metamorphism on the palaeo-Pacific Margin: Journal of Metamorphic Geology, v. 21, p. 299–313, doi:10.1046/j.1525-1314.2003.00443.x.

Hollis, J.A., Clarke, G.L., Klepeis, K.A., Daczko, N.R., and Ireland, T.R., 2004, The regional significance of Cretaceous magmatism and metamorphism in Fiordland, New Zealand, from U-Pb zircon geochronology: Journal of Metamorphic Geology, v. 22, p. 607–627, doi:10.1111/j.1525-1314.2004.00537.x.

Hout, C., Stowell, H.H., Schwartz, J.J., and Klepeis, K., 2012, New $^{206}Pb/^{238}U$ zircon ages record magmatism and metamorphism in the crustal root of a magmatic arc, Fiordland, New Zealand: Geological Society of America Abstracts with Programs, v. 44, no. 7, p. 586.

Kay, S.M., Godoy, E., and Kurtz, A., 2005, Episodic arc migration, crustal thickening, subduction erosion, and magmatism in the south-central Andes: Geological Society of America Bulletin, v. 117, p. 67–88, doi:10.1130/B25431.1.

Kern, J.M., de Silva, S.L., Schmitt, A.K., Kaiser, J.F., Iriarte, A.R., and Economos, R., 2016, Geochronological imaging of an episodically constructed subvolcanic batholith: U-Pb in zircon chronochemistry of the Altiplano-Puna Volcanic Complex of the Central Andes: Geosphere, doi:10.1130/GES01258.1.

Kimbrough, D.L., Tulloch, A.J., Geary, E., Coombs, D.S., and Landis, C.A., 1993, Isotopic ages from the Nelson region of South Island New Zealand: Crustal structure and definition of the Median Tectonic Zone: Tectonophysics, v. 225, p. 433–448, doi:10.1016/0040-1951(93)90308-7.

Kimbrough, D.L., Tulloch, A.J., Coombs, D.S., Landis, C.A., Johnston, M.R., and Mattinson, J.M., 1994, Uranium-lead zircon ages from the Median Tectonic Zone, New Zealand: New Zealand Journal of Geology and Geophysics, v. 37, p. 393–419, doi:10.1080/00288306.1994.9514630.

Kimbrough, D.L., Smith, D.P., Mahoney, J.B., Moore, T.E., Grove, M., Gastil, R.G., Ortega-Rivera, A., and Fanning, C.M., 2001, Forearc-basin sedimentary response to rapid Late Cretaceous batholith emplacement in the Peninsular Ranges of southern and Baja California: Geology, v. 29, p. 491–494, doi:10.1130/0091-7613(2001)029<0491:FBSRTR>2.0.CO;2.

King, D.S., Klepeis, K.A., Goldstein, A.G., Gehrels, G.E., and Clarke, G.L., 2008, The initiation and evolution of the transpressional Straight River shear zone, central Fiordland, New Zealand: Journal of Structural Geology, v. 30, p. 410–430, doi:10.1016/j.jsg.2007.12.004.

Klepeis, K.A., Clarke, G.L., Gehrels, G., and Vervoort, J., 2004, Processes controlling vertical coupling and decoupling between the upper and lower crust of orogens: Results from Fiordland, New Zealand: Journal of Structural Geology, v. 26, p. 765–791, doi:10.1016/j.jsg.2003.08.012.

Klepeis, K.A., King, D., De Paoli, M., Clarke, G.L., and Gehrels, G., 2007, Interaction of strong lower and weak middle crust during lithospheric extension in western New Zealand: Tectonics, v. 26, TC4017, doi:10.1029/2006TC002003.

Klepeis, K.A., Schwartz, J., Stowell, H., and Tulloch, A., 2016, Gneiss domes, vertical and horizontal mass transfer, and the initiation of extension in the hot lower crustal root of a continental arc, Fiordland, New Zealand: Lithosphere, v. 8, p. 116–140, doi:10.1130/L490.1.

Lackey, J.S., Valley, J.W., Chen, J.H., and Stockli, D.F., 2008, Dynamic magma systems, crustal recycling, and alteration in the central Sierra Nevada Batholith: The oxygen isotope record: Journal of Petrology, v. 49, p. 1397–1426, doi:10.1093/petrology/egn030.

Lee, C.T.A., and Anderson, D.L., 2015, Continental crust formation at arcs, the arclogite "delamination" cycle, and one origin for fertile melting anomalies in the mantle: Science Bulletin, v. 60, p. 1141–1156, doi:10.1007/s11434-015-0828-6.

Little, T.A., Mortimer, N., and McWilliams, M., 1999, An episodic Cretaceous cooling model for the Otago-Marlborough Schist, New Zealand, based on $^{40}Ar/^{39}Ar$ white mica ages: New Zealand Journal of Geology and Geophysics, v. 42, p. 305–325, doi:10.1080/00288306.1999.9514848.

Ludwig, K.R., 2012, Isoplot 3.75, a geochronological toolkit for Excel, Berkeley Geochronology Center Special Publication No. 5, p. 75.

Marcotte, S.B., Klepeis, K.A., Clarke, G.L., Gehrels, G., and Hollis, J.A., 2005, Intra-arc transpression in the lower crust and its relationship to magmatism in a Mesozoic magmatic arc: Tectonophysics, v. 407, p. 135–163, doi:10.1016/j.tecto.2005.07.007.

Mattinson, J.M., Kimbrough, D.L., and Bradshaw, J.Y., 1986, Western Fiordland orthogneiss: Early Cretaceous arc magmatism and granulite facies metamorphism, New Zealand: Contributions to Mineralogy and Petrology, v. 92, p. 383–392, doi:10.1007/BF00572167.

Matzel, J.E.P., Bowring, S.A., and Miller, R.B., 2006, Time scales of pluton construction at differing crustal levels: Examples from the Mount Stuart and Tenpeak intrusions, North Cascades, Washington: Geological Society of America Bulletin, v. 118, p. 1412–1430, doi:10.1130/B25923.1.

McCoy-West, A., Mortimer, N., and Ireland, T.R., 2014, U-Pb geochronology of Permian plutonic rocks, Longwood Range, New Zealand: Implications for Median Batholith–Brook Street terrane relations: New Zealand Journal of Geology and Geophysics, v. 57, p. 65–85, doi:10.1080/00288306.2013.869235.

McCulloch, M.T., Bradshaw, J.Y., and Taylor, S.R., 1987, Sm-Nd and Rb-Sr isotopic and geochemical systematics in Phanerozoic granulites from Fiordland, southwest New Zealand: Contributions to Mineralogy and Petrology, v. 97, p. 183–195, doi:10.1007/BF00371238.

Memeti, V., Paterson, S., Matzel, J., Mundil, R., and Okaya, D., 2010, Magmatic lobes as "snapshots" of magma chamber growth and evolution in large, composite batholiths: An example from the Tuolumne intrusion, Sierra Nevada, California: Geological Society of America Bulletin, v. 122, p. 1912–1931, doi:10.1130/B30004.1.

Milan, L.A., Daczko, N.R., Clarke, G.L., and Allibone, A.H., 2016, Complexity of in-situ zircon U-Pb-Hf isotope systematics during arc magma genesis at the roots of a Cretaceous arc, Fiordland, New Zealand: Lithos, v. 264, p. 296–314, doi:10.1016/j.lithos.2016.08.023.

Miller, R., Paterson, S., and Matzel, J., 2009, Plutonism at different crustal levels: Insights from the ~5–40 km (paleodepth) North Cascades crustal section, Washington, *in* Miller, R.B., and Snoke, A.W., eds., Crustal cross sections from the western North American Cordillera and elsewhere: Implications for tectonic and petrologic processes: Geological Society of America Special Paper 456, p. 125–149, doi:10.1130/2009.2456(05).

Mortimer, N., 2004, New Zealand's geological foundations: Gondwana Research, v. 7, p. 261–272, doi:10.1016/S1342-937X(05)70324-5.

Mortimer, N., 2008, Zealandia, *in* Spencer, J.E., and Titley, S.R., eds., Ores and orogenesis: Circum-Pacific tectonics, geologic evolution, and ore deposits: Arizona Geological Society Digest 22, p. 227–233.

Mortimer, N., and Campbell, H., 2014, Zealandia: Our continent revealed: Rosedale, Auckland, Penguin Random House New Zealand, 272 p.

Mortimer, N., Tulloch, J., Spark, R.N., Walker, N.W., Ladley, E., Allibone, A., and Kimbrough, D.L., 1999, Overview of the Median Batholith, New Zealand: A new interpretation of the geology of the Median Tectonic Zone and adjacent rocks: Journal of African Earth Sciences, v. 29, p. 257–268, doi:10.1016/S0899-5362(99)00095-0.

Mortimer, N., et al., 2014, High-level stratigraphic scheme for New Zealand rocks: New Zealand Journal of Geology and Geophysics, v. 57, p. 402–419, doi:10.1080/00288306.2014.946062.

Muir, R.J., Weaver, S.D., Bradshaw, J.D., Eby, G.N., and Evans, J.A., 1995, The Cretaceous Separation Point batholith, New Zealand: Granitoid magmas formed by melting of mafic lithosphere: Journal of the Geological Society [London], v. 152, p. 689–701, doi:10.1144/gsjgs.152.4.0689.

Muir, R.J., Ireland, T.R., Weaver, S.D., Bradshaw, J.D., Evans, J.A., Eby, G.N., and Shelley, D., 1998, Geochronology and geochemistry of a Mesozoic magmatic arc system, Fiordland, New Zealand: Journal of the Geological Society [London], v. 155, p. 1037–1053, doi:10.1144/gsjgs.155.6.1037.

Oliver, G.J.H., 1976, High grade metamorphic rocks of Doubtful Sound, Fiordland, New Zealand: A study of the lower crust [Ph.D. thesis]: Dunedin, New Zealand, University of Otago, 547 p.

Oliver, G.J.H., 1977, Feldspathic hornblende and garnet granulites and associated anorthosite pegmatites from Doubtful Sound, Fiordland, New Zealand: Contributions to Mineralogy and Petrology, v. 65, p. 111–121, doi:10.1007/BF00371051.

Oliver, G.J.H., 1980, Geology of the granulite and amphibolite facies gneisses of Doubtful Sound, Fiordland, New Zealand: New Zealand Journal of Geology and Geophysics, v. 23, p. 27–41, doi:10.1080/00288306.1980.10424190.

Paterson, S.R., and Ducea, M.N., 2015, Arc magmatic tempos: Gathering the evidence: Elements, v. 11, p. 91–98, doi:10.2113/gselements.11.2.91.

Paterson, S.R., Miller, R.B., Alsleben, H., Whitney, D.L., Valley, P.M., and Hurlow, H., 2004, Driving mechanisms for >40 km of exhumation during contraction and extension in a continental arc, Cascades core, Washington: Tectonics, v. 23, TC3005, doi:10.1029/2002TC001440.

Paterson, S.R., Okaya, D., Memeti, V., Economos, R., and Miller, R.B., 2011, Magma addition and flux calculations of incrementally constructed magma chambers in continental margin arcs: Combined field, geochronologic, and thermal modeling studies: Geosphere, v. 7, p. 1439–1468, doi:10.1130/GES00696.1.

Pepper, M., Gehrels, G., Pullen, A., Ibanez-Mejia, M., Ward, K.M., and Kapp, P., 2016, Magmatic history and crustal genesis of western South America: Constraints from U-Pb ages

and Hf isotopes of detrital zircons in modern rivers: Geosphere, v. 12, p. 1532–1555, doi: 10.1130/GES01315.1.

Ramezani, J., and Tulloch, A.J., 2009, TIMS U-Pb geochronology of southern and eastern Fiordland: http://data.gns.cri.nz/paperdata/index.jsp, doi: 10.21420/G2CC7Z.

Ramos, V.A., 2009, Anatomy and global context of the Andes: Main geologic features and the Andean orogenic cycle, *in* Kay, S.M., et al., eds., Backbone of the Americas: Shallow subduction, plateau uplift, and ridge and terrane collision: Geological Society of America Memoir 204, p. 31–65, doi:10.1130/2009.1204(02).

Ramos, V.A., Litvak, V.D., Folguera, A., and Spagnuolo, M., 2014, An Andean tectonic cycle: From crustal thickening to extension in a thin crust (34°–37°SL): Geoscience Frontiers, v. 5, p. 351–367, doi:10.1016/j.gsf.2013.12.009.

Rubatto, D., 2002, Zircon trace element geochemistry: Partitioning with garnet and the link between U-Pb ages and metamorphism: Chemical Geology, v. 184, p. 123–138, doi: 10.1016/S0009-2541(01)00355-2.

Sagar, M., Palin, J., Tulloch, A., and Heath, L., 2016, The geology, geochronology and affiliation of the Glenroy Complex and adjacent plutonic rocks, southeast Nelson: New Zealand Journal of Geology and Geophysics, v. 59, p. 213–235, doi:10.1080/00288306.2015.1101004.

Sambridge, M.S., and Compston, W., 1994, Mixture modeling of multi-component data sets with application to ion-probe zircon ages: Earth and Planetary Science Letters, v. 128, p. 373–390, doi:10.1016/0012-821X(94)90157-0.

Schwartz, J.J., John, B.E., Cheadle, M.J., Wooden, J.L., Mazdab, F., Swapp, S., and Grimes, C.B., 2010, Dissolution-reprecipitation of igneous zircon in mid-ocean ridge gabbro, Atlantis Bank, Southwest Indian Ridge: Chemical Geology, v. 274, p. 68–81, doi:10.1016/j.chemgeo.2010.03.017.

Schwartz, J.J., Stowell, H.H., Klepeis, K.A., Tulloch, A.J., Kylander-Clark, A.R.C., Hacker, B.R., and Coble, M.A., 2016, Thermochronology of extensional orogenic collapse in the deep crust of Zealandia: Geosphere, v. 12, p. 647–677, doi:10.1130/GES01232.1.

Scott, J.M., and Palin, J.M., 2008, LA-ICP-MS U-Pb zircon ages from Mesozoic plutonic rocks in eastern Fiordland, New Zealand: New Zealand Journal of Geology and Geophysics, v. 51, p. 105–113, doi:10.1080/00288300809509853.

Scott, J.M., Turnbull, I.M., Ewing, T.A., Allibone, A.H., Palin, J.M., and Cooper, A.F., 2008, Petrology and geochronology of the volcaniclastic and volcanogenic Mesozoic Loch Burn Formation in eastern Fiordland, New Zealand: New Zealand Journal of Geology and Geophysics, v. 51, p. 89–103, doi:10.1080/00288300809509852.

Scott, J.M., Cooper, A.F., Palin, J.M., Tulloch, A.J., Kula, J., Jongens, R., Spell, T.L., and Pearson, N.J., 2009, Tracking the influence of a continental margin on growth of a magmatic arc, Fiordland, New Zealand, using thermobarometry, thermochronology, and zircon U-Pb and Hf isotopes: Tectonics, v. 28, TC6007, doi:10.1029/2009TC002489.

Scott, J.M., Cooper, A.F., Tulloch, A.J., and Spell, T.L., 2011, Crustal thickening of the Early Cretaceous paleo-Pacific Gondwana margin: Gondwana Research, v. 20, p. 380–394, doi: 10.1016/j.gr.2010.10.008.

Shea, E.K., Miller, J.S., Miller, R.B., Bowring, S.A., and Sullivan, K.M., 2016, Growth and maturation of a mid- to shallow-crustal intrusive complex, North Cascades, Washington: Geosphere, v. 12, p. 1489–1516, doi:10.1130/GES01290.1.

Spell, T.L., McDougall, I., and Tulloch, A.J., 2000, Thermochronologic constraints on the breakup of the Pacific Gondwana margin: The Paparoa metamorphic core complex, South Island, New Zealand: Tectonics, v. 19, p. 433–451, doi:10.1029/1999TC900046.

Stowell, H.H., Klepeis, K., Schwartz, J.J., Tulloch, A., and Parker, K., 2013, Granulite-facies metamorphism and the initiation of intraplate extension in the lower crust of a continental magmatic arc, Fiordland, New Zealand: Geological Society of America Abstracts with Programs, v. 45, no. 7, p. 799.

Stowell, H., Parker, K.O., Gatewood, M., Tulloch, A., and Koenig, A., 2014, Temporal links between pluton emplacement, garnet granulite metamorphism, partial melting and extensional collapse in the lower crust of a Cretaceous magmatic arc, Fiordland, New Zealand: Journal of Metamorphic Geology, v. 32, p. 151–175, doi:10.1111/jmg.12064.

Sutherland, R., and Melhuish, A., 2000, Formation and evolution of the Solander Basin, southwestern South Island, New Zealand, controlled by a major fault in continental crust and mantle: Tectonics, v. 19, p. 44–61, doi:10.1029/1999TC900048.

Tulloch, A.J., and Challis, G.A., 2000, Emplacement depths of Paleozoic Mesozoic plutons from western New Zealand estimated by hornblende Al geobarometry: New Zealand Journal of Geology and Geophysics, v. 43, p. 555–567, doi:10.1080/00288306.2000.9514908.

Tulloch, A.J., and Kimbrough, D., 2003, Paired plutonic belts in convergent margins and the development of high Sr/Y magmatism: Peninsular Ranges batholith of Baja-California and Median batholith of New Zealand, *in* Johnson, S.E., et al., eds., Tectonic evolution of northwestern Mexico and the southwestern USA: Geological Society of America Special Paper 374, p. 275–296, doi:10.1130/0-8137-2374-4.275.

Tulloch, A.J., Ireland, T.R., Kimbrough, D.L., Griffin, W.L., and Ramezani, J., 2011, Autochthonous inheritance of zircon through Cretaceous partial melting of Carboniferous plutons: The Arthur River Complex, Fiordland, New Zealand: Contributions to Mineralogy and Petrology, v. 161, p. 401–421, doi: 10.1007/s00410-010-0539-6.

Turnbull, I.M., Anderson, H.J., and Uruski, C.I., 1993, Cretaceous and Cenozoic sedimentary basins of Western Southland, South Island, New Zealand: New Zealand Institute of Geological and Nuclear Sciences Monograph 1 (New Zealand Geological Survey Basin Studies 4), 86 p.

Turnbull, I.M., Allibone, A.H., and Jongens, R., 2010, Geology of the Fiordland area: Lower Hutt, New Zealand Institute of Geological and Nuclear Sciences, 97 p., scale 1:250,000.

Voice, P.J., Kowalewski, M., and Eriksson, K.A., 2011, Quantifying the timing and rate of crustal evolution: Global compilation of radiometrically dated detrital zircon grains: Journal of Geology, v. 119, p. 109–126, doi:10.1086/658295.

Whitney, D.L., and Evans, B.W., 2010, Abbreviations for names of rock-forming minerals: American Mineralogist, v. 95, p. 185–187, doi:10.2138/am.2010.3371.

MANUSCRIPT RECEIVED 16 AUGUST 2016
REVISED MANUSCRIPT RECEIVED 1 NOVEMBER 2016
MANUSCRIPT ACCEPTED 15 DECEMBER 2016

Printed in the USA